Cell

Distinct Factors Control Histone Variant H3.3 Localization at Specific Genomic Regions

Aaron D. Goldberg,[1] Laura A. Banaszynski,[1,15] Kyung-Min Noh,[1,15] Peter W. Lewis,[1] Simon J. Elsaesser,[1] Sonja Stadler,[1] Scott Dewell,[2] Martin Law,[4] Xingyi Guo,[11] Xuan Li,[3] Duancheng Wen,[5,6,7] Ariane Chapgier,[8] Russell C. DeKelver,[9] Jeffrey C. Miller,[9] Ya-Li Lee,[9] Elizabeth A. Boydston,[9] Michael C. Holmes,[9] Philip D. Gregory,[9] John M. Greally,[12,13] Shahin Rafii,[5,6,7] Chingwen Yang,[3] Peter J. Scambler,[8] David Garrick,[4] Richard J. Gibbons,[4] Douglas R. Higgs,[4] Ileana M. Cristea,[10] Fyodor D. Urnov,[9] Deyou Zheng,[11,13,14,*] and C. David Allis[1,*]

[1]Laboratory of Chromatin Biology and Epigenetics
[2]Genomics Resource Center
[3]Gene Targeting Resource Center
The Rockefeller University, 1230 York Avenue, New York, NY 10065, USA
[4]MRC Molecular Haematology Unit, Weatherall Institute of Molecular Medicine, John Radcliffe Hospital, Headington, Oxford OX3 9DS, UK
[5]Howard Hughes Medical Institute
[6]Ansary Stem Cell Institute
[7]Department of Genetic Medicine
Weill Cornell Medical College, New York, NY 10065, USA
[8]Molecular Medicine Unit, Institute of Child Health, 30 Guilford Street, London WC1N 1EH, UK
[9]Sangamo BioSciences, Point Richmond Tech Center, 501 Canal Boulevard, Suite A100, Richmond, CA 94804, USA
[10]Department of Molecular Biology, Princeton University, Princeton, NJ 08544, USA
[11]Department of Neurology
[12]Department of Medicine
[13]Department of Genetics
[14]Department of Neuroscience
Albert Einstein College of Medicine, Bronx, NY 10461, USA
[15]These authors contributed equally to this work
*Correspondence: deyou.zheng@einstein.yu.edu (D.Z.), alliscd@rockefeller.edu (C.D.A.)
DOI 10.1016/j.cell.2010.01.003

SUMMARY

The incorporation of histone H3 variants has been implicated in the epigenetic memory of cellular state. Using genome editing with zinc-finger nucleases to tag endogenous H3.3, we report genome-wide profiles of H3 variants in mammalian embryonic stem cells and neuronal precursor cells. Genome-wide patterns of H3.3 are dependent on amino acid sequence and change with cellular differentiation at developmentally regulated loci. The H3.3 chaperone Hira is required for H3.3 enrichment at active and repressed genes. Strikingly, Hira is not essential for localization of H3.3 at telomeres and many transcription factor binding sites. Immunoaffinity purification and mass spectrometry reveal that the proteins Atrx and Daxx associate with H3.3 in a Hira-independent manner. Atrx is required for Hira-independent localization of H3.3 at telomeres and for the repression of telomeric RNA. Our data demonstrate that multiple and distinct factors are responsible for H3.3 localization at specific genomic locations in mammalian cells.

INTRODUCTION

Genetic and biochemical evidence have recently converged to connect epigenetic mechanisms at the level of chromatin (Bernstein et al., 2007; Goldberg et al., 2007; Henikoff, 2008). In addition to nucleosome remodeling and covalent modifications, eukaryotic cells generate variation in chromatin by the introduction of variant histone proteins (Henikoff, 2008). Mammalian cells express three major types of noncentromeric histone H3 variants, H3.1, H3.2, and H3.3 (Hake and Allis, 2006; Hake et al., 2006). Although histone H3.3 differs from H3.2 and H3.1 at only four or five amino acids (Figure S1A available online), H3.3 is specifically enriched at transcriptionally active genes and regulatory elements in nonpluripotent cells (Ahmad and Henikoff, 2002; Jin et al., 2009; Mito et al., 2005, 2007).

Histone H3.3 is incorporated into chromatin in both a replication-coupled (RC) and replication-independent (RI) manner, while the incorporation of H3.2 is coupled to replication (Ahmad and Henikoff, 2002; De Koning et al., 2007). The histone chaperone CAF-1 is found in a complex with H3.1 and mediates RC nucleosome assembly (Smith and Stillman, 1989; Tagami et al., 2004). In contrast, the histone chaperone Hira has been found in a complex with H3.3 and mediates RI nucleosome assembly (Ray-Gallet et al., 2002; Tagami et al., 2004).

Hira has been implicated in H3.3-specific deposition and chromatin assembly (Loyola and Almouzni, 2007). Although Hira is required for chromatin assembly and H3.3 deposition in the male pronucleus of *Drosophila*, Hira is not required for global H3.3 deposition in *Drosophila* embryos or adult cells, suggesting that alternate pathways may mediate H3.3 nucleosome assembly (Bonnefoy et al., 2007; Loppin et al., 2005). Indeed, the chromatin remodeling factor CHD1 was shown to physically associate with Hira and has been suggested to work with Hira to mediate H3.3 incorporation into chromatin in *Drosophila* (Konev et al., 2007).

In *Drosophila*, both Hira and H3.3 are required for fertility and for transcriptional regulation of specific genes, but not for developmental viability (Bonnefoy et al., 2007; Hödl and Basler, 2009; Nakayama et al., 2007; Sakai et al., 2009). However, in mice, targeted mutagenesis of Hira results in a more severe phenotype, with gastrulation defects leading to early embryonic lethality (Roberts et al., 2002). Given the conserved association between H3.3 and active chromatin, H3.3 has been speculated to play an important role in mammalian embryonic stem cells (ESCs) (Creyghton et al., 2008; Gaspar-Maia et al., 2009). However, no genome-wide studies in pluripotent cells distinguish between H3 variants, nor do they examine the genome-wide role of Hira or other histone chaperones in specifying H3.3 localization at specific genomic regions.

Here, we report genome-wide profiles of histone H3 variant localization in mammalian ESCs and neuronal precursor cells (NPCs), and we establish the dependence and independence of these patterns on Hira. We find that Hira is required for genome-wide H3.3 enrichment at active and repressed genes in ESCs. Surprisingly, H3.3 enrichment at many transcription factor binding sites (TFBS) and telomeres is *Hira independent*. To identify factors that might mediate specific Hira-independent localization of H3.3, we use immunoprecipitation and mass spectrometry. We identify Atrx and Daxx as proteins that specifically associate with H3.3 in both pluripotent and nonpluripotent cells, both in the presence and in the absence of Hira. Unlike Hira, Atrx is not required for H3.3 localization at genes or TFBS. However, Atrx is specifically required for enrichment of H3.3 at telomeres in ESCs, and for the repression of telomeric RNA.

RESULTS

Genome-wide Patterns of H3.3 Enrichment Are Dependent upon Endogenous Amino Acid Sequence

To distinguish H3 variants in our study without altering endogenous levels of H3 variant expression, we used designed zinc-finger nucleases (ZFNs) (Carroll, 2008) in both gene addition (Moehle et al., 2007) and correction (Urnov et al., 2005) modes to engineer a panel of heterozygous ESC lines carrying one allele of wild-type H3.3B and another allele of H3.3B with a C-terminal EYFP tag (H3.3-EYFP), HA tag (H3.3-HA), or H3.3B with an epitope tag and simultaneous mutation toward H3.2 or H3.1 (H3.2-EYFP, H3.1-EYFP, H3.2-HA, and H3.1S31-HA) (Figure S1). All heterozygously tagged ESCs retain three ''wild-type'' copies of H3.3 genes, including one copy of unmodified H3.3B (Figure S1G), and two copies of H3.3A. Western blots demonstrate equal protein expression in the epitope-tagged H3 variant ESC lines (Figure S1H).

To assess the genome-wide localization of histone H3 variants at high resolution, we used chromatin immunoprecipitation followed by massively parallel sequencing (ChIP-seq) (Barski et al., 2007; Mikkelsen et al., 2007). We found 10,099 total genic and intergenic regions highly enriched for H3.3 in crosslinking ChIP-seq of ESCs, in contrast to 1442 regions enriched for H3.2, and we observe that gene-rich regions of the genome show greater enrichment of H3.3 than H3.2 (Figures 1A and 1B). On a chromosomal scale map, H3.3 enrichment correlates with markers of transcription, including Ser-5 phosphorylated RNA polymerase II (RNAPII), H3K4me3, H3K36me3, and H3K4me1 (Figure 1A). Unbiased clustering analyses confirm the genome-wide correlation of H3.3 with active histone modifications, particularly H3K4me1 (Table S1). Despite different epitope tags, we found extremely similar profiles of H3.3-HA and H3.3-EYFP (Figure 1A, Table S1, Figures S2A and S2B). Genome-wide analysis also reveals specific enrichment of H3.3 at previously identified genic and intergenic ESC TFBS (Chen et al., 2008), as well as peaks of H3.3 in specific unannotated intergenic regions (Figure 1B).

To analyze H3 variant enrichment in different classes of repeats, we determined the relative enrichment of specific repeat sequences from our ChIP-seq experiments and compared it to that from control input DNA. H3.3 was reproducibly depleted in satellite repeat sequences and in Y-chromosomal repeat DNA (Figure 1C). We found the most significant enrichment of H3.3 in the (TTAGGG)n repeat that is the conserved telomeric DNA sequence among vertebrates (Meyne et al., 1989) (Figure 1C). This telomeric enrichment of H3.3 is consistent with telomeric foci of incorporation visible on the largely heterochromatic Y chromosome (Figures S1J–S1O), and with a recent report of telomeric localization of transfected epitope-tagged H3.3 in ESCs (Wong et al., 2009). Mutation of H3.3B to H3.2 or H3.1S31 alters genome-wide patterns of H3.3 enrichment, demonstrating that the amino acid sequence of an endogenous H3.3 gene determines its genomic localization in mammalian cells.

H3.3 Is Enriched at TSS of Active and Repressed HCP Genes, and in the Bodies and TES of Transcribed Sequences

As there has been some disagreement regarding the patterns of H3.3 at active versus repressed genes in vertebrates (Jin and Felsenfeld, 2006; Jin et al., 2009; Sutcliffe et al., 2009; Tamura et al., 2009), we used ChIP-seq to address the genome-wide patterns of H3 variant enrichment around gene transcription start sites (TSS) in mouse ESCs. We find that H3.3 is not exclusively a marker of transcriptionally active genes in ESCs and NPCs.

Previous studies show that the majority of genes with high CpG content promoters (HCP genes) in both ESCs and differentiated cells are marked by histone H3K4me3 and the presence of RNAPII, regardless of whether the gene is active or repressed (Barski et al., 2007; Guenther et al., 2007; Mikkelsen et al., 2007). When we divide HCP genes into low, medium, and high expression in ESCs (see the Experimental Procedures), we find that H3.3, like H3K4me3 and RNAPII, is enriched around the

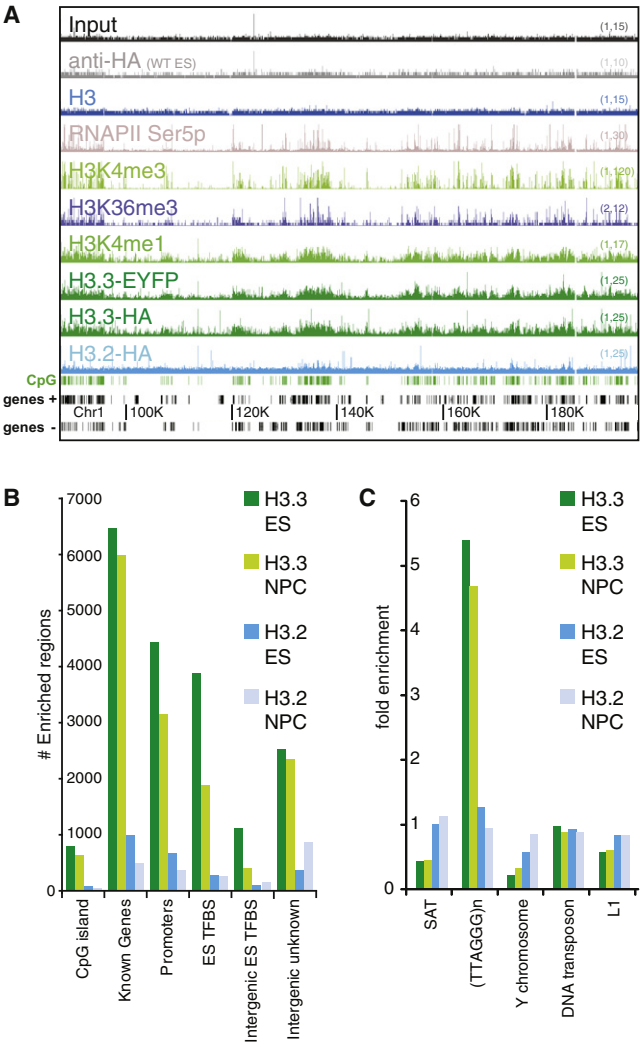

Figure 1. Genomic Localization of Histone H3.3 Is Dependent on Amino Acid Sequence

(A) ChIP-seq profiles across 120 MB of chromosome 1 in mouse ESCs, with antibodies as indicated. The y axis represents the number of reads spanning a genomic position [scale on right (baseline, maximum)]. CpG islands (green) and genes [refseq (+) and refseq (−)] are shown below plots. Data for general H3 in ESCs are from Mikkelsen et al. (2007).

(B) Annotations of H3 variant enriched regions. The y axis is the number of enriched regions identified for each H3 variant, while the x axis represents different categories of gene annotation and ESC TFBS (defined in Chen et al., 2008).

(C) Association of H3.3 with repetitive elements. Data are presented as fold enrichment over input. SAT, satellite repeats; (TTAGGG)n, telomeric DNA repeats.

See Figure S1 for details of ZFN-mediated generation and characterization of ESC lines and Table S1 for genome-wide correlation of ChIP-seq data sets.

TSS of both active and repressed genes (Figure 2A). In both native and crosslinking ChIP-seq, we find H3.3 less enriched at the TSS itself (Figures 2A and 2D, Figures S2A–S2D). This depletion of the −1 nucleosome at the TSS of active and inactive genes (Schones et al., 2008) has been attributed both to the instability of nucleosomes containing H3.3 and H2A.Z and to the presence of specific sequences at CpG promoters that directly reduce nucleosome stability (Jin et al., 2009; Ramirez-Carrozzi et al., 2009).

More than one-fifth of HCP genes in ESCs carry both H3K4me3 and H3K27me3 in their promoters, and these transcriptionally repressed "bivalent" genes are proposed to represent genes that are poised for activation after cell differentiation (Bernstein et al., 2006; Mikkelsen et al., 2007). When we analyze the pattern of H3 variants at bivalent TSS by ChIP-seq, we find that H3.3 is enriched around the TSS of bivalent genes in ESCs, while mutation of H3.3 toward H3.2 or H3.1 abolishes this enrichment (Figure 2G, Figure S3).

Although H3.3 is incorporated around the TSS of both active and repressed genes in ESCs, H3.3 is enriched in the body of active genes, but not that of repressed genes (Figures 2A, 2G, and 2H, Figures S2A–S2D). Mononucleosome resolution analysis indicates that H3.3 is incorporated into the +1 nucleosomes in both active and repressed genes, but up to +3 nucleosomes and further into the coding regions of active genes (Figures S2Q–S2W). The level of H3.3 in gene bodies is correlated with gene expression, particularly at highly expressed genes (Spearman's rank correlation coefficient $\rho = 0.54$, $p < 2.2e\text{-}16$; see Figure 2A and Figure S2). Upon mutation of H3.3 to H3.2 or H3.1S31, H3.3 specific patterns of enrichment around the TSS and gene body are lost, generating patterns similar to general H3 (Figures 2B and 2D).

In accordance with previous studies (Henikoff et al., 2009; Jin et al., 2009; Mito et al., 2005), H3.3 enrichment often extends beyond the gene body and past the transcriptional end site (TES) at highly expressed genes in ESCs (Figures 2A and 2H) and in differentiated NPCs (Figure S2CC). At highly expressed genes such as beta-actin (*Actb*), H3.3 enrichment increases immediately after the TES, and peaks at approximately +700 bp ± 200 bp after the TES (Figure 2H, Figures S2A–S2D). We observe a similar pattern of H3.3 localization in the bodies and after the TES of transcribed noncoding RNA (Guttman et al., 2009) (Figure 2I). Interestingly, the distribution of post-TES peaks of serine-5-phosphorylated RNAPII are closely colocalized with peaks of H3.3 at active genes, with the phosphorylated RNAPII peak slightly downstream (~200 bp) from the H3.3 peak. We did not observe any significant post-TES enrichment of histone modifications that are associated with active genes, such as H3K4me3, H3K4me1, and H3K36me3 (Figures 2E and 2F, Figure S2). Post-TES enrichment of H3.3 is also dependent on amino acid sequence (Figures 2B and 2D, Figure S2). From these analyses, we conclude that H3.3 is localized around the TSS of both active and repressed HCP genes and that both H3.3 and phosphorylated RNAPII are significantly enriched beyond the TES of highly expressed genes in undifferentiated and differentiated mammalian cells.

The Profile of H3.3 at Cell Type-Specific Genes and Regulatory Elements Changes with Cell Differentiation

To determine how genome-wide patterns of H3.3 change with cell differentiation, we differentiated both H3.3-HA and H3.2-HA ESCs to NPCs (Figure S3A) (Conti et al., 2005). In ESCs, H3.3 is

enriched in the bodies of expressed pluripotency genes such as *Esrrb*, *Nanog*, and *Oct4*, correlated with H3K36me3 (Figure 3A, Table S2, Figure S3B). Upon differentiation of ESCs to NPCs, the expression of most pluripotency genes is lost (Conti et al., 2005). Accordingly, the enrichment of H3.3 and H3K36me3 in the bodies of pluripotency genes largely disappears upon cell differentiation (Figure 3A, Figure S3B).

After differentiation of ESCs to NPCs, the profile of H3.3 changes with resolution of bivalent domains. In bivalent ES genes that resolve to H3K4me3 and become transcriptionally active in NPCs, H3.3 is maintained around the TSS and also incorporated into the gene body, in correlation with H3K36me3 and H3K4me1 (Figure 3B, Figure S3C). For example, upon differentiation to NPCs, H3.3 extends into the gene body of the active epidermal growth factor receptor gene *Egfr*, correlating with H3K36me3 and H3K4me1 (Figure 3B). In contrast, for bivalent genes that remain transcriptionally repressed and resolve to either H3K27me3 or no mark in NPCs, H3.3 enrichment is reduced at the TSS upon differentiation (Figure S3C). As expected, H3.2 remains unenriched at the TSS in both ESCs and NPCs (Figure S3C).

While the pattern of H3.3 changes at cell type-specific genes, housekeeping genes that remain highly expressed through differentiation retain similar enriched patterns of H3.3 incorporation. For example, H3.3 remains enriched around the TSS and within the gene body of the housekeeping gene lactate dehydrogenase A *Ldha* (Figure 3C, Figure S3A). In both ESCs and NPCs, we find the greatest enrichment of H3.3 at highly expressed metabolic and housekeeping genes (Figure S3D). Our data show that the overall relationship between H3.3 incorporation and gene expression is retained in ESCs and NPCs, with H3.3 and H3K4 methylation marking the TSS of active and poised HCP genes, and H3.3 enriched in the body and TES of active HCP genes. At cell type-specific genes, H3.3 localization changes with cellular state.

Genome-scale studies have demonstrated that in addition to genes (Mito et al., 2005), H3.3 replacement marks the boundaries of regulatory elements (Jin et al., 2009; Mito et al., 2007). Thirty-six percent (3627) of H3.3 enriched regions in mouse ESCs are located outside of known annotated genes (Figures 1B and 3D–3F). We therefore compared our genome-wide distributions for histone H3 variants in ESCs and NPCs with established genome-wide maps for 13 distinct sequence-specific TFs in ESCs (Chen et al., 2008). We find that H3.3 is enriched genome-wide at genic and intergenic TFBS for all 13 characterized TFs in ESCs (Figure 3D, Figure S3E). Remarkably, 3878 (38%) of the overall regions enriched for H3.3 in ESCs (Figure 1B) correspond to previously identified TFBS (Chen et al., 2008). Again, peaks of H3.3 at TFBS are dependent on H3.3 amino acid sequence (Figures 3D–3G, Figure S3E).

Many of the specific peaks of H3.3 at TFBS are cell-type specific, especially those located in intergenic regions (Figures 1B and 3D–3G, Figure S3B, data not shown). We find that H3.3 incorporation at TFBS bound by multiple TFs increases significantly with the number of bound TFs in ESCs, but these same elements do not show increased H3.3 in NPCs (Figure 3F, Figure S3F). Genomic locations bound by more than four TFs are called multiple transcription factor-binding loci (MTL), and a subset of MTL bound by Oct4-Sox2-Nanog have been shown to serve as ESC-specific enhanceosomes (Chen et al., 2008). For example, an intergenic region near the AP-2 transcription factor gene *Tcfap2c* is a target for multiple transcription factors in ESCs (Chen et al., 2008). We find H3.3 enriched at this region specifically in ESCs, with enrichment lost in NPCs (Figure 3F).

After differentiation to NPCs, genome-wide enrichment of H3.3 at ESC TFBS is reduced, but not eliminated (Figure 3E, Figure S3E). At some specific TFBS (Figure 3F), H3.3 and H3K4me1 enrichment is lost upon differentiation to NPCs. However, at other TFBS, such as those 5′ and 3′ of *Nanog*, H3.3 and H3K4me1 enrichment is reduced but partially maintained (Figure S3B). H3K4me1 and H3.3 have been separately shown to significantly colocalize with TFBS and other regulatory elements (Heintzman et al., 2007; Mito et al., 2007; Wang et al., 2008), but the patterns of H3.3 and H3K4me1 have never been directly compared. In our analysis, 26% of H3K4me1 peaks overlap with H3.3 peaks, and peaks of H3.3 are five times more likely to be associated with peaks of H3K4me1 than H3K4me3 (Table S1, $p < 0.00001$). In addition to ESC-specific intergenic peaks of H3.3 and H3K4me1 (Figure 3F), we also found 724 intergenic peaks of H3.3 and H3K4me1 that are specific to differentiated NPCs and that do not correspond to any known TFBS (Figure 3G, data not shown). It is possible that these represent uncharacterized cell type-specific enhancers. Overall, our data demonstrate that the genome-wide localization of H3.3 changes with cell differentiation at cell type-specific genes and regulatory elements.

Hira Is Required for Enrichment of H3.3 at Active and Repressed Genes

After establishing genome-wide patterns of H3.3 in undifferentiated ESCs and differentiated NPCs, we sought to determine whether these patterns were dependent on the H3.3 chaperone Hira. We therefore used ZFNs to tag one allele of the endogenous H3.3B gene in Hira$^{-/-}$ ESCs (Meshorer et al., 2006; Roberts et al., 2002) with a C-terminal EYFP tag (Figure 4A, Figure S4A), and compared the genome-wide localization of H3.3-EYFP in the presence and absence of Hira.

Using native ChIP-seq, we find that Hira is required for genome-wide H3.3 enrichment at active and repressed HCP genes (Figures 4B–4G). In the absence of Hira, the pattern of H3.3 around active and repressed genes resembles H3.2, with no enrichment surrounding the TSS, and depletion of H3.3 at the TSS itself (Figures 4D and 4E). For example, in Hira$^{-/-}$ ESCs, the enrichment of H3.3 around the TSS of the repressed bivalent gene *Pparg* is abolished (Figure 4F). At highly expressed housekeeping genes such as the ribosomal protein-coding gene *Rps19*, the gene body and post-TES enrichment of H3.3 is similarly decreased in the absence of Hira (Figure 4G). Our data demonstrate that the vast majority of H3.3 enrichment at both active and repressed genes in ESCs is Hira dependent.

One possible explanation for the loss of H3.3 localization at active and repressed genes in Hira$^{-/-}$ ESCs is a significant alteration in patterns of gene expression. Remarkably, microarray analysis reveals that global patterns of ESC gene expression are maintained in Hira$^{-/-}$ ESCs (Figures S4B–S4D). Moreover, genome-wide patterns of H3K36me3 are extremely similar in

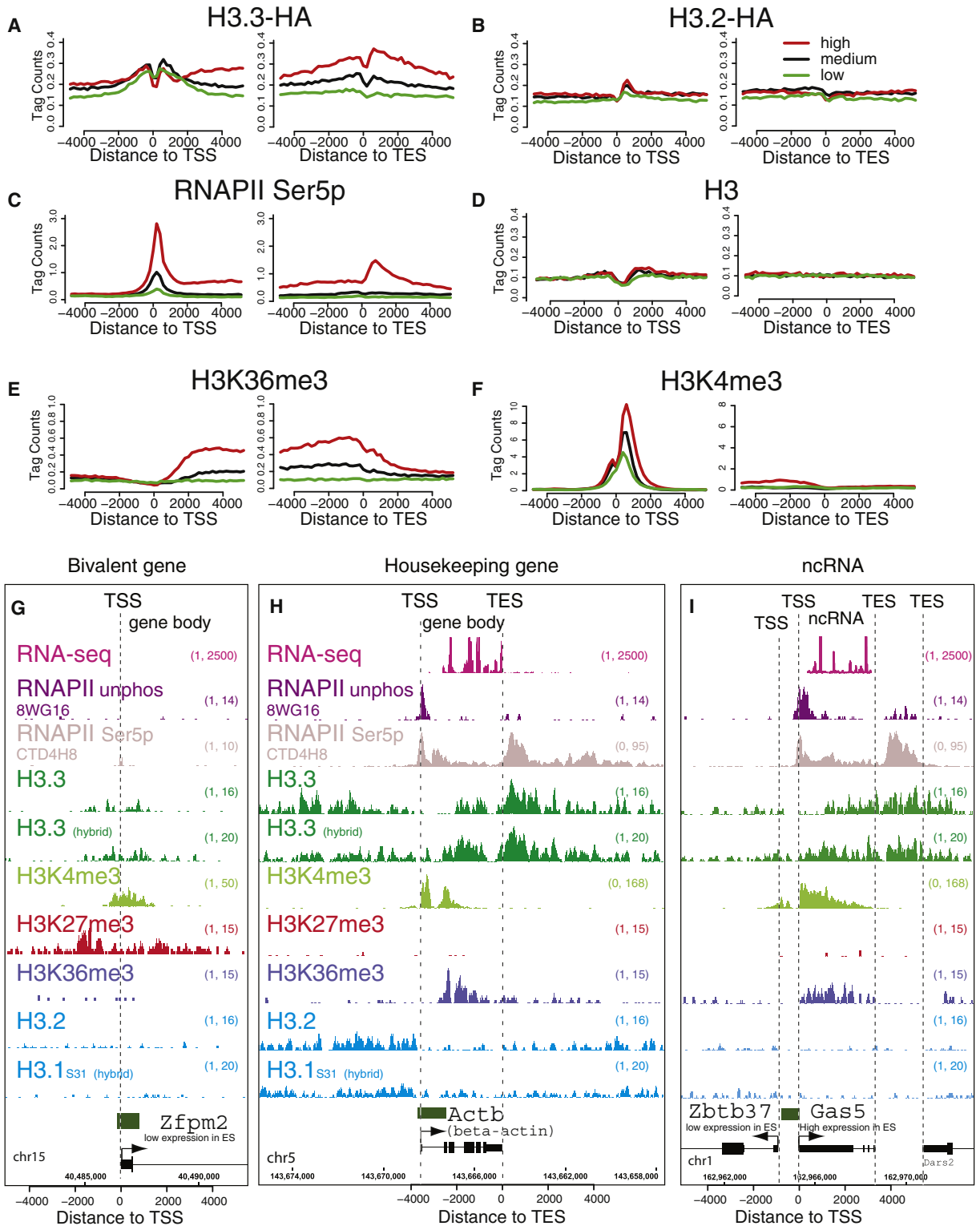

Figure 2. Specific Patterns of H3.3 and Phosphorylated RNA Polymerase at Active and Repressed Genes

(A–F) Profiles of H3 variants, H3, H3 modifications, or RNAPII as indicated above each panel across the TSS and TES for highly active (red), medium expressing (black), or low expressing (green) CpG-rich genes in ESCs. The y axis represents the average number of tags per gene per 200 bp per 1,000,000 mapped reads. H3 data are from Mikkelsen et al. (2007). (A)–(E) are from crosslinking ChIP-seq, while (F) is from native ChIP-seq.

(G) H3.3 is enriched around the TSS, but not into the gene body of the H3K4me3/H3K27me3 bivalent and transcriptionally repressed *Zfpm2* gene in ESCs.

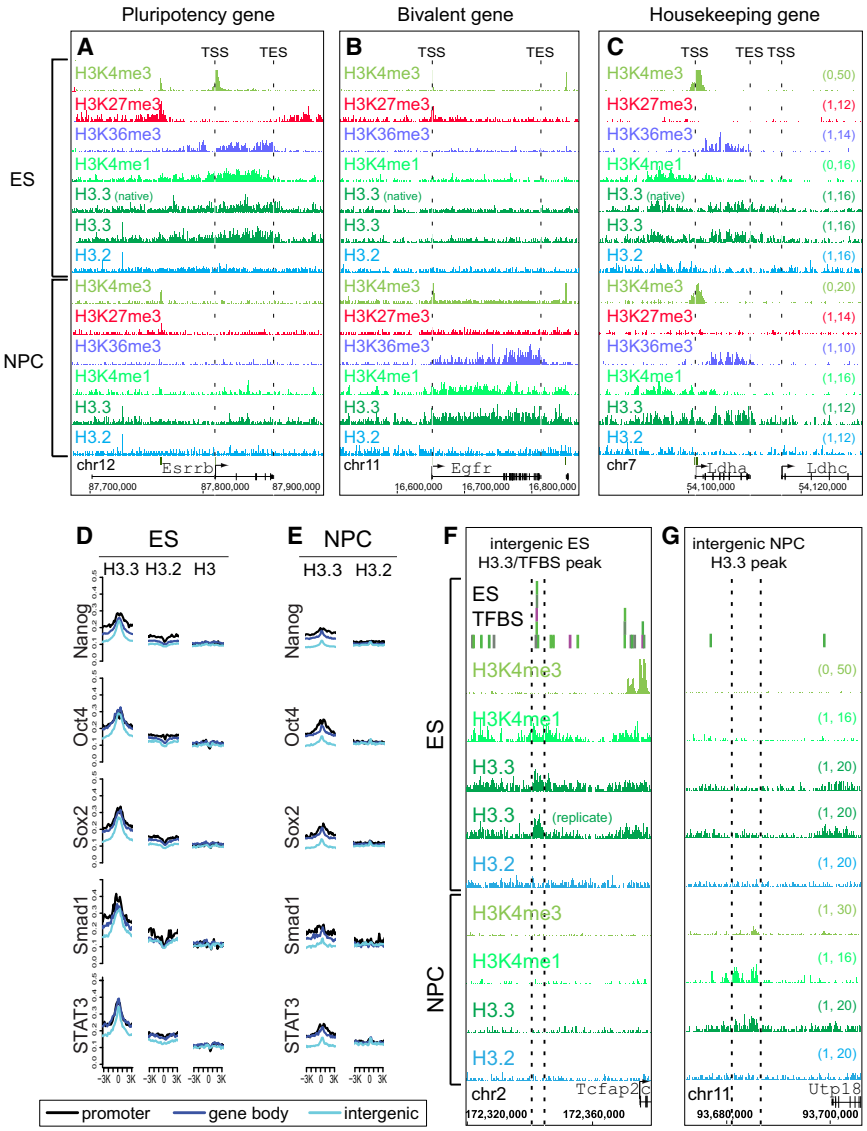

Figure 3. Cell Type-Specific Enrichment of H3.3 at Transcription Factor Binding Sites and Developmentally Regulated Genes

(A) H3.3, H3K4me1, and H3K36me3 are enriched in the gene body of the highly expressed pluripotency gene *Esrrb* in ESCs, and this enrichment is largely lost upon differentiation to NPCs.

(B) The epidermal growth factor receptor gene *Egfr* is H3K4me3/H3K27me3 bivalent and transcriptionally repressed in ESCs. Upon differentiation to NPCs, H3.3, H3K4me1, and H3K36me3 are enriched in the *Egfr* gene body.

(C) H3.3, H3K4me1, and H3K36me3 are enriched in the gene body of the housekeeping gene lactate dehydrogenase A *Ldha* in both ESCs and NPCs and is not enriched in the neighboring *Ldhc* gene.

(D and E) H3.3 is enriched genome-wide around ESC TFBS. Crosslinking ChIP-seq genome-wide profiles of H3 variants as indicated around ESC binding sites for Nanog, Oct4, Sox2, Smad1, and STAT3. TFBS in mouse ESCs were from a previous ChIP-seq study (Chen et al., 2008), and classified as promoter (black), gene body (dark blue), or intergenic (light blue). (D) represents data from ESCs, while (E) represents data from NPCs at identical regions. The y axis represents number of tags per binding site per 200 bp per 1,000,000 mapped reads. Data for H3 in ESCs are from (Mikkelsen et al., 2007).

(F) H3.3 and H3K4me1 are enriched at an intergenic region bound by multiple transcription factors (Chen et al., 2008) specifically in ESCs.

(G) H3.3 and H3K4me1 are enriched at an intergenic region specifically in NPCs.

The y axes in (A)–(C) are identical (indicated in the right side of C). In (A)–(E), "(native)" indicates native H3.3-HA ChIP-seq, and "(replicate)" indicates biological replicate H3.3-HA ChIP-seq from F1 hybrid ESC background. See also Figure S3.

wild-type and Hira$^{-/-}$ ESCs (Figures S4E–S4H). This result is similar to the recent observation that global patterns of ESC gene expression are maintained following knockdown of CHD1 (Gaspar-Maia et al., 2009). We conclude that genome-wide enrichment of H3.3 at active and repressed genes is Hira dependent but is not required for maintenance of the undifferentiated ESC transcriptome.

Hira-Independent Enrichment of H3.3 at Transcription Factor Binding Sites

We next examined the Hira dependence of H3.3 enrichment at genic and intergenic TFBS. Surprisingly, global H3.3 profiles are largely maintained at ESC TFBS in Hira$^{-/-}$ ESCs (Figure 5A, Figure S5, Table S3), indicating that H3.3 enrichment at most known regulatory elements is Hira independent. For example, H3.3 enrichment at an intergenic MTL approximately 30 kb from the *Mmp17* gene is maintained in Hira$^{-/-}$ ESCs (Figure 5B), as is H3.3 enrichment at an intergenic MTL near the repressed *Foxi3* gene (Figure 5C). Indeed, levels of H3.3 are increased at some TFBS in Hira$^{-/-}$ ESCs (Figure S5A). However, levels of H3.3 are also reduced at other TFBS in Hira$^{-/-}$ ESCs (Table S3, Figure S5B). Of all previously identified ESC TFBS (Chen et al., 2008), 34% show greater than 2-fold more H3.3 tags in Hira$^{+/+}$ than in Hira$^{-/-}$, while 12% show greater than 2-fold more H3.3

(H) H3.3 and RNAPII Ser5p are enriched in the gene body and after the TES of the highly expressed gene *Actb* (beta-actin) in ESCs. Data for the RNAPII unphos 8WG16 track are from Mikkelsen et al. (2007). RNA-seq data are from Cloonan et al. (2008).

(I) H3.3 is enriched around the TSS and into the body of the noncoding RNA gene *Gas5*, but less enriched in the gene body of the neighboring low expressing *Zbtb37* gene in ESCs. Data are represented as in Figure 1A. Gene is shown to scale below plot, with start and direction or transcription indicated by arrow. Green rectangles above the gene represent CpG islands.

In (G)–(I), hybrid indicates F1 hybrid ES background. See also Figure S2.

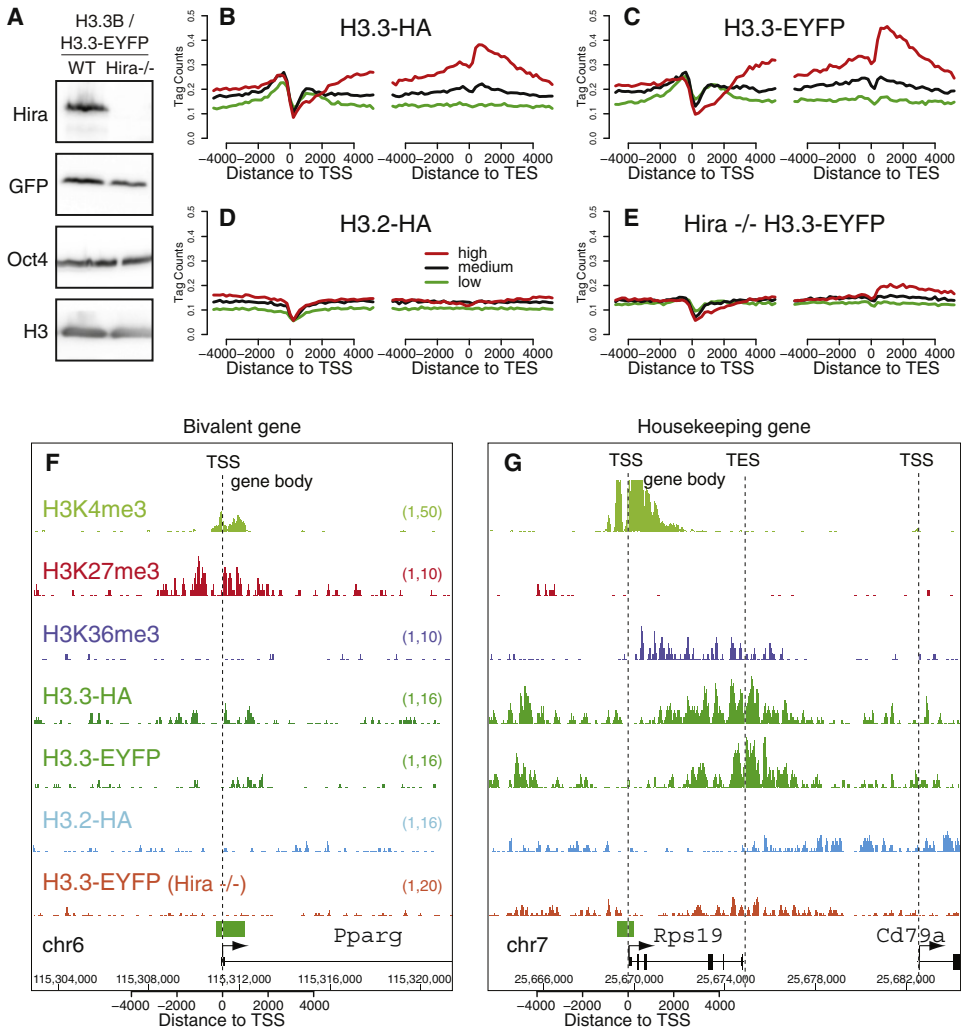

Figure 4. Enrichment of H3.3 at Active and Repressed Genes Is Hira Dependent

(A) Immunoblots showing expression of H3.3-EYFP in wild-type and Hira$^{-/-}$ ESCs, with antibodies as indicated.

(B–E) Native ChIP-seq profiles of H3 variants, in wild-type ESCs (B–D) and Hira$^{-/-}$ ESCs (E) across the TSS and TES for highly active (red), medium expressing (black), or low expressing (green) CpG-rich genes, with data represented as in Figure 2. See also Figure S4.

(F) H3.3 enrichment at the TSS of repressed bivalent gene *Pparg* is Hira dependent.

(G) H3.3 enrichment at the active, ribosomal-protein coding gene *Rps19* is Hira dependent.

tags in Hira$^{-/-}$, indicating that targeting of H3.3 to the majority (54%) of known ESC TFBS is Hira independent (Table S3, Figure S5). Global profiles of H3K4me1 are very similar in wild-type and Hira$^{-/-}$ ESCs (Figures S4E, S4F, and S5D), indicating that Hira is also not required to maintain the localization of H3K4me1. Overall, these data demonstrate that Hira is not essential for the localization of H3.3 at many TFBS in mammalian ESCs.

Hira-Independent Association of Atrx and Daxx with Histone H3.3

To identify candidates that might mediate Hira-independent localization of H3.3, we used immunoaffinity purification and mass spectrometry (Cristea et al., 2005) (Figure 6A, Figure S6). We found many interacting proteins common to all H3 variants in wild-type and Hira$^{-/-}$ ESCs, including core histones and previously described members common to both RC and RI chromatin assembly complexes, such as Nasp, Asf1a, Asf1b, and Rbap48 (see Table S4). Notably, the previously described H3.3 chaperone Hira (Tagami et al., 2004) was identified specifically in proteins isolated with H3.3 (Figures 6A and 6B).

In addition to Hira, we also identified Atrx and Daxx as proteins that specifically associate with H3.3 (Figures 6A and 6B). Atrx is a member of the SNF2 family of chromatin remodeling factors (Picketts et al., 1996). Mutations of human ATRX give rise to the ATR-X syndrome, a disorder characterized by a form of X-linked mental retardation that is frequently associated with alpha thalassemia (Gibbons et al., 2008). ATRX coexists in a chromatin-remodeling complex with the death domain-associated protein Daxx, and these proteins localize to heterochromatin and

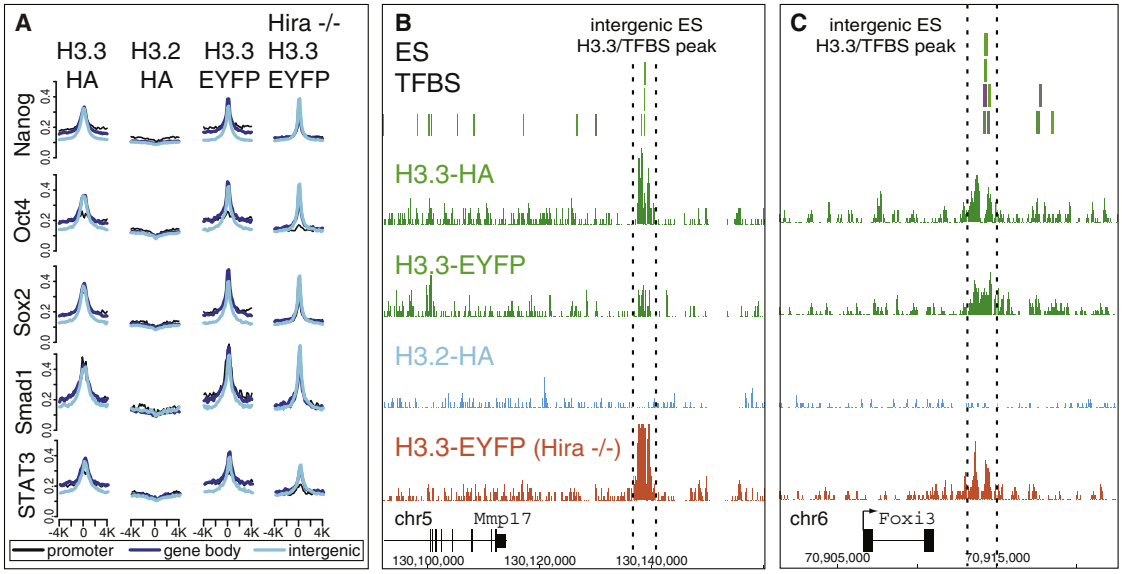

Figure 5. Hira Is Not Essential for H3.3 Enrichment at Transcription Factor Binding Sites

(A) Native ChIP-seq genome-wide profiles of H3.3 around previously described ESC TFBS (Chen et al., 2008), with data analyzed as in Figure 3.

(B and C) Localization of H3.3 in ESCs at intergenic enhancer elements near *Mmp17* (B) and *Foxi3* (C) is Hira independent.

See also Figure S5 and Table S3.

promyelocytic leukemia (PML) nuclear bodies in human and mouse cells (Tang et al., 2004; Xue et al., 2003). As Atrx and Daxx specifically associate with H3.3 in both wild-type and Hira$^{-/-}$ ESCs, we conclude that this association is Hira independent.

To determine whether the association between H3.3, Atrx, and Daxx was conserved in differentiated human cells, we isolated oligonucleosomes and chromatin-associated proteins from HeLa cells stably expressing FLAG-HA tagged H3.3 or H3.1 (Tagami et al., 2004) (Figures 6C and 6D). After FLAG affinity purification, immunoblots of H3.3- and H3.1-associated proteins reveal that both Daxx and Atrx are specifically associated with H3.3 but not H3.1 oligonucleosomes in human cells (Figure 6E).

Atrx Is Required to Maintain H3.3 Localization at Telomeres and for Repression of Telomeric Repeat-Containing RNA in ESCs

To determine whether Atrx is required for H3.3 localization, we again used ZFNs to knock in an epitope tag into the endogenous allele of H3.3B, generating heterozygous H3.3B/H3.3B-EYFP in *Atrx*^{flox} and *Atrx*^{null} mouse ESCs (Garrick et al., 2006) (Figure 7A). We then used native ChIP-seq to generate genome-wide profiles of H3.3 in the presence and absence of Atrx. We find that Atrx is not required for H3.3 incorporation at active or repressed genes, or at regulatory elements (Figures S5A and S7A–S7E), as genome-wide profiles of H3.3 are similar at genes and TFBS in *Atrx*^{flox} and *Atrx*^{null} ESCs. Strikingly, both ChIP-seq (Figure 7B) and cell imaging analysis (Figure 7C) demonstrate that Atrx, but not Hira, is specifically required for H3.3 enrichment at telomeres. In accordance with the requirement of Atrx for telomeric localization of H3.3, ChIP analysis shows that Atrx itself is physically associated with telomeres in *Atrx*^{flox} ESCs (Figure 7D).

To investigate the functional consequences of Atrx deletion and the loss of Atrx-dependent telomeric enrichment of H3.3, we examined the chromatin state and transcriptional output of ESC telomeres. The chromatin of ESC and induced pluripotent cell telomeres has previously been shown to have lower levels of the heterochromatin marker H3K9me3 and increased transcription of telomeric repeat-containing RNA (TERRA) in comparison to differentiated cells (Marion et al., 2009). In particular, TERRA has recently been identified as a component of telomeric heterochromatin, and levels of TERRA have been shown to be regulated by chromatin modifying enzymes (Azzalin et al., 2007; Luke and Lingner, 2009; Schoeftner and Blasco, 2008). ChIP of H3K4me3 and H3K9me3 does not show a significant difference in telomeric enrichment between *Atrx*^{flox} and *Atrx*^{null} ESCs (Figure S7F). However, northern blots from *Atrx*^{flox}, *Atrx*^{null}, and *Atrx*^{flox} ESCs 4 days after treatment with Cre reveal reproducible (~1.7-fold) upregulation of TERRA in the absence of Atrx (Figures 7E–7G). Our data demonstrate that Atrx is required for Hira-independent localization of H3.3 at telomeres and for repression of TERRA.

DISCUSSION

In this study, we examine H3 variant localization in mammalian ESCs and differentiated NPCs. Genome-wide patterns of H3.3 are dependent on H3.3-specific amino acid sequence; the enrichment of H3.3 at cell type-specific genes and TFBS is dependent on cellular state. We describe three general categories of H3.3 enrichment in mammalian cells: (1) genes and other transcribed nonrepetitive sequences, (2) TFBS, and

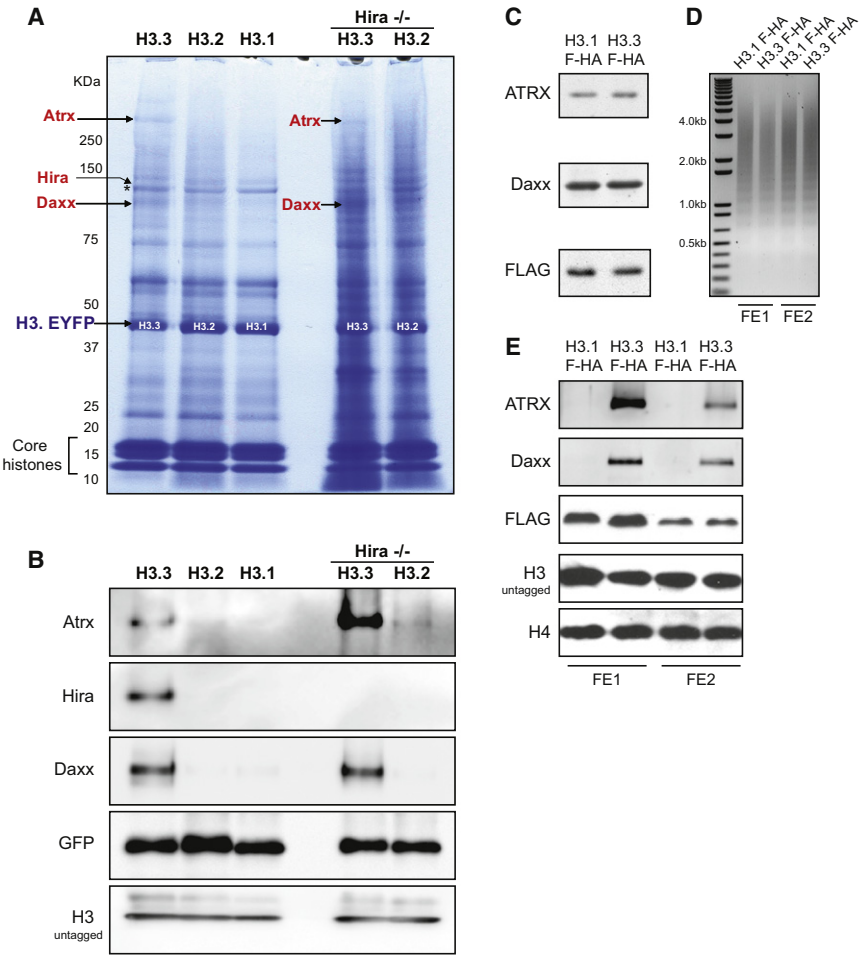

Figure 6. Atrx and Daxx Association with H3.3 Is Specific, Hira Independent, and Conserved in Mouse and Human Cells

(A) H3.3-EYFP, H3.2-EYFP, H3.1-EYFP, and Hira$^{-/-}$ H3.3-EYFP associated proteins were immunopurified from heterozygous H3.3B ESCs via the EYFP tag, resolved by SDS-PAGE, and visualized by Coomassie blue. Proteins were identified by mass spectrometry, and those listed in red are specific to H3.3. The arrow indicating Hira points to a polypeptide in the H3.3 lane running immediately above the polypeptide Nasp (*), which is common to all purified H3 variants. A full list of identified proteins is presented in Table S4.

(B) Immunoblots of immunopurified H3 variant associated proteins from ESCs with antibodies as indicated. See also Figure S6.

(C) Immunoblots of Atrx, Daxx, and FLAG-HA-H3 from HeLa cells stably expressing H3.3-FLAG-HA (FHA) or H3.1-FHA (Tagami et al., 2004).

(D) Oligonucleosomes purified from H3.3-FHA and H3.1-FHA HeLa cells. Micrococcal nuclease digested chromatin was incubated with M2 agarose beads in order to purify H3.3-FHA and H3.1-FHA oligonucleosomes and associated proteins.

(D and E) Two adjacent FLAG elution fractions (FE1 and FE2) from each H3.3-FHA and H3.1-FHA purification are shown. Oligonucleosomal DNA was purified and run on a 1% agarose gel, with fragment size indicated.

(E) Immunoblots of eluate from two adjacent FLAG elution fractions (FE1 and FE2) after FLAG affinity purification from H3.3-FHA and H3.1-FHA oligonucleosomes (D).

(3) telomeres. Remarkably, we find that each of these general categories of H3.3 enrichment in ESCs is mediated by distinct mechanisms. As expected, Hira is required for genic enrichment of H3.3. Unexpectedly, localization of H3.3 at specific TFBS and telomeres is Hira independent, and we have identified Atrx as required for H3.3 localization at telomeres. Our results demonstrate that distinct factors control H3.3 localization at specific genomic locations in mammalian cells.

We find that H3.3 is constitutively enriched around the TSS of active and repressed HCP genes in mammalian ESCs and NPCs, including the TSS of repressed bivalent genes in ESCs. Although a recent genome-wide study found that H3.3 is unenriched at the TSS of repressed genes in HeLa cells (Jin et al., 2009), these results are not necessarily in conflict with our findings. Low CpG content promoter (LCP) and HCP genes have been described to display distinct modes of regulation (Mikkelsen et al., 2007; Ramirez-Carrozzi et al., 2009; Saxonov et al., 2006). Most HCP genes show evidence of transcriptional initiation, assemble unstable nucleosomes, and do not require SWI/SNF nucleosome remodeling complexes for gene induction, while LCP genes assemble stable nucleosomes and require SWI/SNF (Guenther et al., 2007; Ramirez-Carrozzi et al., 2009). Less differentiated cells such as ESCs contain large numbers of HCP genes with characteristics of transcriptional initiation (Guenther et al., 2007; Mikkelsen et al., 2007). Indeed, nearly all (99%) of HCP genes are marked by H3K4me3 in mouse ESCs, whether they are transcriptionally active or repressed (Mikkelsen et al., 2007). In contrast to HCP genes, we do not observe any significant pattern of H3.3 enrichment at LCP genes in ESCs and NPCs (data not shown). Our results are therefore consistent with a model in which H3K4 methylation and H3.3 localization at HCP TSS are coupled to transcriptional initiation.

We find that enrichment of H3.3 in the gene body and after the TES is proportional to transcriptional activity. As with previous studies in *Drosophila* and human cells (Henikoff et al., 2009; Jin et al., 2009; Mito et al., 2005), we find peaks of H3.3 after the TES of highly active genes, and we observe that these peaks are closely paralleled by peaks of Ser-5 phosphorylated RNAPII itself. We demonstrate that chromatin-based "transcriptional punctuation" (Siegel et al., 2009; Talbert and Henikoff, 2009) by H3.3 and phosphorylated RNAPII marks the boundaries of highly expressed genes in both undifferentiated and differentiated mammalian cells, calling attention to a potentially more universal mechanism for histone variant utilization as a genomic "boundary marker."

Our study provides a genome-wide analysis of a histone variant in the presence and absence of a mammalian histone chaperone. We find that H3.3 enrichment at active and

repressed genes is dependent on the histone chaperone Hira. Previous studies suggest that H3.3 deposition in actively transcribed gene bodies may be coupled to transcription, potentially mediated by factors associated with elongating polymerase (Daury et al., 2006; Janicki et al., 2004; Schwartz and Ahmad, 2005). Our data are consistent with Hira-dependent transcription-coupled deposition of H3.3 at transcribed nonrepetitive sequences.

Intriguingly, we do not observe significant abnormalities in Hira$^{-/-}$ ESCs, despite a global lack of H3.3 enrichment at active and repressed genes and despite the requirement of Hira for early embryonic development (Roberts et al., 2002). We speculate that Hira$^{-/-}$ ESCs may be rescued by the replication-coupled deposition of histones during the frequent S phases of rapidly dividing ESCs (Burdon et al., 2002). Hira$^{-/-}$ ESCs divide as rapidly as wild-type ESCs and show a similar preponderance of cells in S phase (A.C. and P.J.S., unpublished data). Overall, our data are consistent with a role for Hira in genic deposition of H3.3.

H3.3 enrichment has recently been shown at TFBS in *Drosophila* and human cells (Jin et al., 2009; Mito et al., 2007). Deposition of H3.3 at TFBS may serve as a mechanism for the maintenance of regulatory elements in a more accessible chromatin conformation (Henikoff, 2008). Close comparison of our data to a recent data set of 13 different TFs in mouse ESCs (Chen et al., 2008) shows H3.3 enriched in ESCs at all known types of TFBS genome-wide, whether in gene bodies, promoters, or intergenic regions. We also find a strong positive correlation between MTL and H3.3 localization, indicating particular enrichment of H3.3 at enhancer elements. Our data demonstrate that Hira is involved in H3.3 localization at some genic and intergenic TFBS. However, we also find that genome-wide H3.3 enrichment at many regulatory elements is Hira independent and Atrx independent. Our data therefore suggest that H3.3 localization at TFBS may be mediated by multiple and distinct factors, including Hira, with as yet unidentified factors mediating H3.3 localization at specific regulatory elements.

We find that H3.3 is specifically enriched in the canonical (TTAGGG)n repeat that is the hallmark of telomeres in vertebrates (Meyne et al., 1989). Previous immunofluorescence studies localizing GFP-tagged Hira to telomeres suggested that Hira facilitates H3.3 deposition at this location (Wong et al., 2009). However, using genome-wide ChIP-seq and cell imaging analyses in Hira$^{-/-}$ ESCs, we show that localization of H3.3 at telomeres in ESCs is Hira independent. Further, we identify Atrx and Daxx as proteins that associate with H3.3 nucleosomes in the presence and absence of Hira.

Recent studies have shown that the *Drosophila* homolog of Atrx, XNP, colocalizes with H3.3 at sites of nucleosome replacement on polytene chromosomes but is not required for H3.3 localization at these sites (Schneiderman et al., 2009). We find that Atrx is required for enrichment of H3.3 at mammalian ESC telomeres, suggesting a divergence of homolog function. Moreover, we demonstrate that in the absence of Atrx, ESCs show upregulation of TERRA. Could ATRX and Daxx serve as specific H3.3 variant deposition machinery for specialized regions of heterochromatin? The ATRX/Daxx complex has previously been shown to have chromatin remodeling activity (Tang et al., 2004; Xue et al., 2003), and we show that Atrx is physically associated with ESC telomeres. In addition to telomeres, our preliminary studies indicate that Atrx is also required for H3.3 enrichment at ribosomal DNA (data not shown), another transcribed repetitive element with characteristics of heterochromatin (McStay and Grummt, 2008).

Our findings raise multiple questions. What is the function of H3.3 at genes, TFBS, and telomeres? Do cellular requirements for H3.3 differ in dividing versus postmitotic cells, where replication-independent deposition might play a larger role? Is Atrx-mediated localization of H3.3 also replication independent, like Hira, or does it occur during replication? Broadly, our study raises the prospect that distinct, region-specific chaperone and remodeling complexes may mediate the localization of a single histone variant (H3.3) to particular genomic regions. Although key factors required for region-specific H3.3 localization have now been identified, the exact deposition mechanisms at play remain an important challenge for future work.

EXPERIMENTAL PROCEDURES

ESC Culture and Differentiation

Mouse ESCs were cultured under standard conditions and differentiated to NPCs as previously described (Conti et al., 2005). Hira$^{-/-}$, *Atrx*^{flox}, and *Atrx*^{null} ESCs have been described previously (Garrick et al., 2006; Meshorer et al., 2006). For more detail, see the Extended Experimental Procedures.

ZFN Design, Targeting, and Verification

ZFNs directed against the mouse H3.3B gene were designed with an archive of validated two-finger modules (Doyon et al., 2008; Urnov et al., 2005). ESCs were transfected with ZFNs and donor with Amaxa nucleofection. Fluorescent ESC colonies were picked and screened by genomic PCR of H3.3B alleles, sequencing of PCR products, flow cytometry, and Southern blot. For more detail, see the Extended Experimental Procedures.

Cellular Extract Preparation

Whole-cell extracts were prepared by resuspension of cell pellets in SDS-Laemmli sample buffer, followed by brief sonication and boiling.

ChIP and ChIP-Seq

Crosslinking and native ChIP were performed as described (Barski et al., 2007; Lee et al., 2006), with minor modifications as detailed in the Extended Experimental Procedures. ChIP DNA was validated by real-time PCR, prepared for Illumina/Solexa sequencing, and sequenced with the Illumina Genome Analyzer II. The CTD4H8 antibody was raised against a chemically synthesized phospho-Ser 5 peptide sequence from the C-terminal domain (CTD) of the largest RPB1 subunit of RNAPII and has been extensively characterized previously (Stock et al., 2007). Other antibodies and more detailed ChIP-seq methods are described in the Extended Experimental Procedures. ChIP-seq assays performed are listed in Table S5. To confirm telomere enrichment, ChIP DNA from *Atrx*^{flox} and *Atrx*^{null} ESCs was probed with a TTAGGG repeat probe as described (Sfeir et al., 2009).

ChIP-Seq Data Analysis

ChIP-seq or input reads were mapped to the mouse genome (build 37, or mm9) using the ELAND alignment software within the Illumina Analysis Pipeline. Profiles in specific genomic regions were displayed in the Affymetrix Integrated Genome Browser. For analysis of repetitive elements, reads were aligned directly to a library of mouse consensus repetitive sequences (http://www.girinst.org/) and enrichments were computed for ChIP against input samples. For TSS/TES profiling, we segregated reference genes (refSeq) into low, medium, and high expression based on a previous microarray analysis (Mikkelsen et al., 2007). For TFBS profiling, binding sites for 13 TFs in mouse ESCs were obtained from a previous ChIP-seq analysis (Chen et al.,

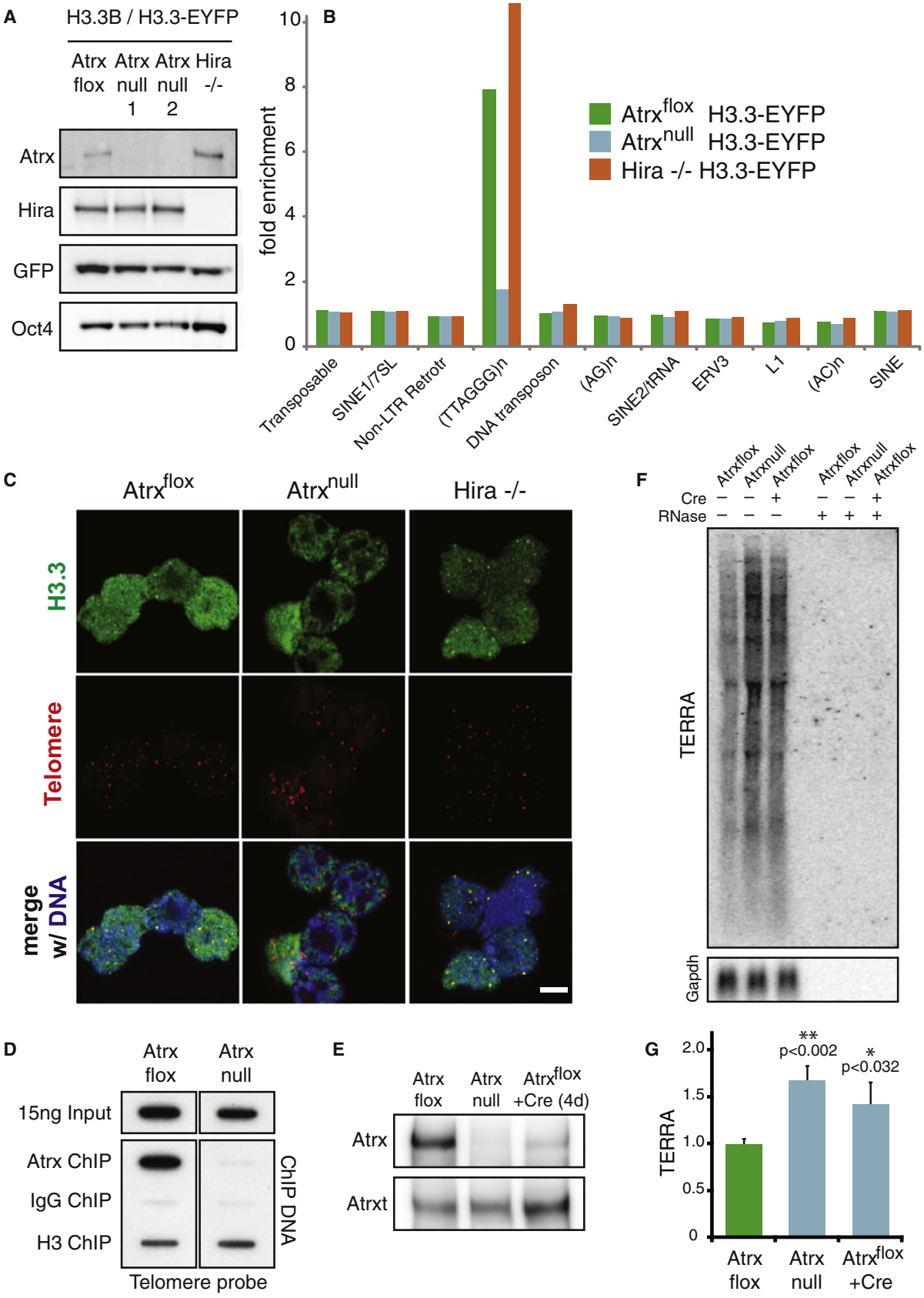
A
H3.3B / H3.3-EYFP
Atrx flox
Atrx null 1
Atrx null 2
Hira -/-
Atrx
Hira
GFP
Oct4
B
fold enrichment
10
8
6
4
2
0
Atrx^flox H3.3-EYFP
Atrx^null H3.3-EYFP
Hira -/- H3.3-EYFP
Transposable
SINE1/7SL
Non-LTR Retrotr
(TTAGGG)n
DNA transposon
(AG)n
SINE2/tRNA
ERV3
L1
(AC)n
SINE
C
Atrx^flox
Atrx^null
Hira -/-
H3.3
Telomere
merge w/ DNA
D
Atrx flox
Atrx null
15ng Input
Atrx ChIP
IgG ChIP
H3 ChIP
ChIP DNA
Telomere probe
E
Atrx flox
Atrx null
Atrx^flox +Cre (4d)
Atrx
Atrxt
F
Atrxflox
Atrxnull
Atrxflox
Atrxflox
Atrxnull
Atrxflox
Cre
RNase
TERRA
Gapdh
G
TERRA
2.0
1.5
1.0
0.5
0
**
p<0.002
*
p<0.032
Atrx flox
Atrx null
Atrx^flox +Cre

2008). To generate density profiles ±5 kb around TSS, TES, bivalent genes, and TFBS, we used a sliding-window method to count the number of ChIP-seq reads in each 200 bp window, and the resulting counts were then normalized by the totals of genes or TFBS and the total mapped reads. For details of data analysis, see the Extended Experimental Procedures.

Gene Expression Analysis of Wild-Type and Hira$^{-/-}$ ESCs

RNA expression data for W9.5 and Hira$^{-/-}$ ESCs was generated from polyA RNA and random primers with the GeneChip Mouse Gene 1.0 ST Array kit (Affymetrix).

Isolation of Protein Complexes and Mass Spectrometric Analysis

Immunoaffinity purifications of EYFP-tagged H3.3, H3.2, H3.1, HIRA$^{-/-}$ H3.3, and HIRA$^{-/-}$ H3.2 were performed as described (Cristea et al., 2005). Matrix-assisted laser desorption/ionization mass spectrometry (MALDI MS) and tandem mass spectrometry (MS/MS) analyses were performed as described (Luo et al., 2009). For more detail, see the Extended Experimental Procedures.

Immunofluorescence and Telomere Fluorescence In Situ Hybridization

Telomere fluorescence in situ hybridization (FISH) of ESCs was performed with a peptide nucleic acid TAMRA-TelG telomere probe (Sfeir et al., 2009), and immunofluorescence was performed with a previously described anti-GFP antibody (Cristea et al., 2005). For more detail, see the Extended Experimental Procedures.

TERRA Analysis

RNA was isolated with RNeasy Mini Kit (QIAGEN), and TERRA analysis was performed as described (Azzalin et al., 2007; Sfeir et al., 2009).

ACCESSION NUMBERS

Our ChIP-seq and microarray data sets have been deposited in the GEO database with accession numbers GSE16893 and GSE19542.

SUPPLEMENTAL INFORMATION

Supplemental Information includes Extended Experimental Procedures, seven figures, and five tables and can be found with this article online at doi:10.1016/j.cell.2010.01.003.

ACKNOWLEDGMENTS

We thank L. Baker, E.M. Duncan, G.G. Wang for critical reading of the manuscript, P. Wu, A. Sfeir, and T. de Lange for telomere reagents and helpful discussion, P.D. Adams for Hira antibodies, R. Jaenisch for F1 hybrid male 129SVJae × *M. m. castaneus* ESCs, G. Almouzni for H3.1 and H3.3-FLAG-HA HeLa cells, K. Zhao for sharing his native ChIP-seq protocol, E. Moehle for drawing the gene editing schemes, N. Jina of the University College London Genomics Core, K.R. Molloy for assistance with mass spectrometric analysis, and S. Mazel and A. North of the Rockefeller University Flow Cytometry and Bio-Imaging Resource Centers. A.D.G. is supported by National Institutes of Health (NIH) Medical Scientist Training Program grant GM07739. L.A.B. is a Damon Runyon Cancer Research Foundation fellow. This work was funded by institutional support from The Rockefeller University and grants from the Tri-Institutional Stem Cell Initiative (funded by the Starr Foundation), Empire State Stem Cell fund through New York State Department of Health contract #C023046, the Howard Hughes Medical Institute (S.R.), Biotechnology and Biological Sciences Research Council UK and the British Heart Foundation (P.J.S.), startup funds from the Albert Einstein College of Medicine of Yeshiva University (D.Z.), and NIH grants RR00862, RR022220, DP1DA026192 (I.M.C.), GM53122, and GM53512 (C.D.A.). J.C.M., M.C.H., Y.L.L., P.D.G., and F.D.U. are full-time employees of Sangamo BioSciences, Inc.

Received: September 9, 2009
Revised: November 23, 2009
Accepted: December 31, 2009
Published: March 4, 2010

REFERENCES

Ahmad, K., and Henikoff, S. (2002). The histone variant H3.3 marks active chromatin by replication-independent nucleosome assembly. Mol. Cell *9*, 1191–1200.

Azzalin, C.M., Reichenbach, P., Khoriauli, L., Giulotto, E., and Lingner, J. (2007). Telomeric repeat containing RNA and RNA surveillance factors at mammalian chromosome ends. Science *318*, 798–801.

Barski, A., Cuddapah, S., Cui, K., Roh, T.Y., Schones, D.E., Wang, Z., Wei, G., Chepelev, I., and Zhao, K. (2007). High-resolution profiling of histone methylations in the human genome. Cell *129*, 823–837.

Bernstein, B.E., Mikkelsen, T.S., Xie, X., Kamal, M., Huebert, D.J., Cuff, J., Fry, B., Meissner, A., Wernig, M., Plath, K., et al. (2006). A bivalent chromatin structure marks key developmental genes in embryonic stem cells. Cell *125*, 315–326.

Bernstein, B.E., Meissner, A., and Lander, E.S. (2007). The mammalian epigenome. Cell *128*, 669–681.

Bonnefoy, E., Orsi, G.A., Couble, P., and Loppin, B. (2007). The essential role of Drosophila HIRA for de novo assembly of paternal chromatin at fertilization. PLoS Genet. *3*, 1991–2006.

Burdon, T., Smith, A., and Savatier, P. (2002). Signalling, cell cycle and pluripotency in embryonic stem cells. Trends Cell Biol. *12*, 432–438.

Carroll, D. (2008). Progress and prospects: zinc-finger nucleases as gene therapy agents. Gene Ther. *15*, 1463–1468.

Chen, X., Xu, H., Yuan, P., Fang, F., Huss, M., Vega, V.B., Wong, E., Orlov, Y.L., Zhang, W., Jiang, J., et al. (2008). Integration of external signaling pathways with the core transcriptional network in embryonic stem cells. Cell *133*, 1106–1117.

Cloonan, N., Forrest, A.R., Kolle, G., Gardiner, B.B., Faulkner, G.J., Brown, M.K., Taylor, D.F., Steptoe, A.L., Wani, S., Bethel, G., et al. (2008). Stem cell

Figure 7. Atrx Is Required for Hira-Independent Enrichment of H3.3 at Telomeres, and for Repression of Telomeric Repeat-Containing RNA

(A) Immunoblots showing expression of H3.3-EYFP in Atrxflox, Atrxnull, and Hira$^{-/-}$ ESCs, with antibodies as indicated.

(B) ChIP-seq analysis of H3.3 enrichment at repetitive elements in Atrxflox, Atrxnull, and Hira$^{-/-}$ ESCs. Fold enrichment of repetitive elements in ChIP-seq data are plotted over input.

(C) Immunofluorescence (IF) and telomere fluorescence in situ hybridization (FISH) of Atrxflox, Atrxnull, and Hira$^{-/-}$ ESCs expressing H3.3B/H3.3-EYFP. Representative confocal images of interphase ESCs demonstrate that H3.3 colocalization with telomeres is lost in Atrxnull ESCs (middle), but maintained in Hira$^{-/-}$ ESCs (right). The scale bar represents 5 μm.

(D) ChIP of Atrx, control IgG, and H3 was performed in Atrxflox and Atrxnull ESCs, followed by slot blot with a telomere probe.

(E) Immunoblots of Atrx in Atrxflox, Atrxnull, and Atrxflox ESCs 4 days after treatment with retroviral Cre. Atrxt refers to a previously identified alternative splicing product of Atrx that remains expressed in Atrxnull ESCs (Garrick et al., 2006).

(F) Representative northern blot for TERRA (upper panel) and Gapdh (lower panel) in Atrxflox and Atrxnull ESCs in the presence and absence of Cre. To ensure that signal is from RNA, we treated samples on the right with RNase for 30 min as indicated.

(G) Quantification of TERRA normalized to Gapdh. Error bars represent the standard deviation of three independent experiments.

See also Figure S7.

transcriptome profiling via massive-scale mRNA sequencing. Nat. Methods *5*, 613–619.

Conti, L., Pollard, S.M., Gorba, T., Reitano, E., Toselli, M., Biella, G., Sun, Y., Sanzone, S., Ying, Q.L., Cattaneo, E., and Smith, A. (2005). Niche-independent symmetrical self-renewal of a mammalian tissue stem cell. PLoS Biol. *3*, e283.

Creyghton, M.P., Markoulaki, S., Levine, S.S., Hanna, J., Lodato, M.A., Sha, K., Young, R.A., Jaenisch, R., and Boyer, L.A. (2008). H2AZ is enriched at polycomb complex target genes in ES cells and is necessary for lineage commitment. Cell *135*, 649–661.

Cristea, I.M., Williams, R., Chait, B.T., and Rout, M.P. (2005). Fluorescent proteins as proteomic probes. Mol. Cell. Proteomics *4*, 1933–1941.

Daury, L., Chailleux, C., Bonvallet, J., and Trouche, D. (2006). Histone H3.3 deposition at E2F-regulated genes is linked to transcription. EMBO Rep. *7*, 66–71.

De Koning, L., Corpet, A., Haber, J.E., and Almouzni, G. (2007). Histone chaperones: an escort network regulating histone traffic. Nat. Struct. Mol. Biol. *14*, 997–1007.

Doyon, Y., McCammon, J.M., Miller, J.C., Faraji, F., Ngo, C., Katibah, G.E., Amora, R., Hocking, T.D., Zhang, L., Rebar, E.J., et al. (2008). Heritable targeted gene disruption in zebrafish using designed zinc-finger nucleases. Nat. Biotechnol. *26*, 702–708.

Garrick, D., Sharpe, J.A., Arkell, R., Dobbie, L., Smith, A.J., Wood, W.G., Higgs, D.R., and Gibbons, R.J. (2006). Loss of Atrx affects trophoblast development and the pattern of X-inactivation in extraembryonic tissues. PLoS Genet. *2*, e58.

Gaspar-Maia, A., Alajem, A., Polesso, F., Sridharan, R., Mason, M.J., Heidersbach, A., Ramalho-Santos, J., McManus, M.T., Plath, K., Meshorer, E., and Ramalho-Santos, M. (2009). Chd1 regulates open chromatin and pluripotency of embryonic stem cells. Nature *460*, 863–868.

Gibbons, R.J., Wada, T., Fisher, C.A., Malik, N., Mitson, M.J., Steensma, D.P., Fryer, A., Goudie, D.R., Krantz, I.D., and Traeger-Synodinos, J. (2008). Mutations in the chromatin-associated protein ATRX. Hum. Mutat. *29*, 796–802.

Goldberg, A.D., Allis, C.D., and Bernstein, E. (2007). Epigenetics: a landscape takes shape. Cell *128*, 635–638.

Guenther, M.G., Levine, S.S., Boyer, L.A., Jaenisch, R., and Young, R.A. (2007). A chromatin landmark and transcription initiation at most promoters in human cells. Cell *130*, 77–88.

Guttman, M., Amit, I., Garber, M., French, C., Lin, M.F., Feldser, D., Huarte, M., Zuk, O., Carey, B.W., Cassady, J.P., et al. (2009). Chromatin signature reveals over a thousand highly conserved large non-coding RNAs in mammals. Nature *458*, 223–227.

Hake, S.B., and Allis, C.D. (2006). Histone H3 variants and their potential role in indexing mammalian genomes: the "H3 barcode hypothesis". Proc. Natl. Acad. Sci. USA *103*, 6428–6435.

Hake, S.B., Garcia, B.A., Duncan, E.M., Kauer, M., Dellaire, G., Shabanowitz, J., Bazett-Jones, D.P., Allis, C.D., and Hunt, D.F. (2006). Expression patterns and post-translational modifications associated with mammalian histone H3 variants. J. Biol. Chem. *281*, 559–568.

Heintzman, N.D., Stuart, R.K., Hon, G., Fu, Y., Ching, C.W., Hawkins, R.D., Barrera, L.O., Van Calcar, S., Qu, C., Ching, K.A., et al. (2007). Distinct and predictive chromatin signatures of transcriptional promoters and enhancers in the human genome. Nat. Genet. *39*, 311–318.

Henikoff, S. (2008). Nucleosome destabilization in the epigenetic regulation of gene expression. Nat. Rev. Genet. *9*, 15–26.

Henikoff, S., Henikoff, J.G., Sakai, A., Loeb, G.B., and Ahmad, K. (2009). Genome-wide profiling of salt fractions maps physical properties of chromatin. Genome Res. *19*, 460–469.

Hödl, M., and Basler, K. (2009). Transcription in the absence of histone H3.3. Curr. Biol. *19*, 1221–1226.

Janicki, S.M., Tsukamoto, T., Salghetti, S.E., Tansey, W.P., Sachidanandam, R., Prasanth, K.V., Ried, T., Shav-Tal, Y., Bertrand, E., Singer, R.H., and Spector, D.L. (2004). From silencing to gene expression: real-time analysis in single cells. Cell *116*, 683–698.

Jin, C., and Felsenfeld, G. (2006). Distribution of histone H3.3 in hematopoietic cell lineages. Proc. Natl. Acad. Sci. USA *103*, 574–579.

Jin, C., Zang, C., Wei, G., Cui, K., Peng, W., Zhao, K., and Felsenfeld, G. (2009). H3.3/H2A.Z double variant-containing nucleosomes mark 'nucleosome-free regions' of active promoters and other regulatory regions. Nat. Genet. *41*, 941–945.

Konev, A.Y., Tribus, M., Park, S.Y., Podhraski, V., Lim, C.Y., Emelyanov, A.V., Vershilova, E., Pirrotta, V., Kadonaga, J.T., Lusser, A., and Fyodorov, D.V. (2007). CHD1 motor protein is required for deposition of histone variant H3.3 into chromatin in vivo. Science *317*, 1087–1090.

Lee, T.I., Johnstone, S.E., and Young, R.A. (2006). Chromatin immunoprecipitation and microarray-based analysis of protein location. Nat. Protoc. *1*, 729–748.

Loppin, B., Bonnefoy, E., Anselme, C., Laurençon, A., Karr, T.L., and Couble, P. (2005). The histone H3.3 chaperone HIRA is essential for chromatin assembly in the male pronucleus. Nature *437*, 1386–1390.

Loyola, A., and Almouzni, G. (2007). Marking histone H3 variants: how, when and why? Trends Biochem. Sci. *32*, 425–433.

Luke, B., and Lingner, J. (2009). TERRA: telomeric repeat-containing RNA. EMBO J. *28*, 2503–2510.

Luo, Y., Li, T., Yu, F., Kramer, T., and Cristea, I.M. (2009). Resolving the composition of protein complexes using a MALDI LTQ Orbitrap. J. Am. Soc. Mass Spectrom. *21*, 34–46.

Marion, R.M., Strati, K., Li, H., Tejera, A., Schoeftner, S., Ortega, S., Serrano, M., and Blasco, M.A. (2009). Telomeres acquire embryonic stem cell characteristics in induced pluripotent stem cells. Cell Stem Cell *4*, 141–154.

McStay, B., and Grummt, I. (2008). The epigenetics of rRNA genes: from molecular to chromosome biology. Annu. Rev. Cell Dev. Biol. *24*, 131–157.

Meshorer, E., Yellajoshula, D., George, E., Scambler, P.J., Brown, D.T., and Misteli, T. (2006). Hyperdynamic plasticity of chromatin proteins in pluripotent embryonic stem cells. Dev. Cell *10*, 105–116.

Meyne, J., Ratliff, R.L., and Moyzis, R.K. (1989). Conservation of the human telomere sequence (TTAGGG)n among vertebrates. Proc. Natl. Acad. Sci. USA *86*, 7049–7053.

Mikkelsen, T.S., Ku, M., Jaffe, D.B., Issac, B., Lieberman, E., Giannoukos, G., Alvarez, P., Brockman, W., Kim, T.K., Koche, R.P., et al. (2007). Genome-wide maps of chromatin state in pluripotent and lineage-committed cells. Nature *448*, 553–560.

Mito, Y., Henikoff, J.G., and Henikoff, S. (2005). Genome-scale profiling of histone H3.3 replacement patterns. Nat. Genet. *37*, 1090–1097.

Mito, Y., Henikoff, J.G., and Henikoff, S. (2007). Histone replacement marks the boundaries of cis-regulatory domains. Science *315*, 1408–1411.

Moehle, E.A., Moehle, E.A., Rock, J.M., Rock, J.M., Lee, Y.L., Lee, Y.L., Jouvenot, Y., Jouvenot, Y., DeKelver, R.C., Dekelver, R.C., et al. (2007). Targeted gene addition into a specified location in the human genome using designed zinc finger nucleases. Proc. Natl. Acad. Sci. USA *104*, 3055–3060.

Nakayama, T., Nishioka, K., Dong, Y.X., Shimojima, T., and Hirose, S. (2007). Drosophila GAGA factor directs histone H3.3 replacement that prevents the heterochromatin spreading. Genes Dev. *21*, 552–561.

Picketts, D.J., Higgs, D.R., Bachoo, S., Blake, D.J., Quarrell, O.W., and Gibbons, R.J. (1996). ATRX encodes a novel member of the SNF2 family of proteins: mutations point to a common mechanism underlying the ATR-X syndrome. Hum. Mol. Genet. *5*, 1899–1907.

Ramirez-Carrozzi, V.R., Braas, D., Bhatt, D.M., Cheng, C.S., Hong, C., Doty, K.R., Black, J.C., Hoffmann, A., Carey, M., and Smale, S.T. (2009). A unifying model for the selective regulation of inducible transcription by CpG islands and nucleosome remodeling. Cell *138*, 114–128.

Ray-Gallet, D., Quivy, J.P., Scamps, C., Martini, E.M., Lipinski, M., and Almouzni, G. (2002). HIRA is critical for a nucleosome assembly pathway independent of DNA synthesis. Mol. Cell *9*, 1091–1100.

Roberts, C., Sutherland, H.F., Farmer, H., Kimber, W., Halford, S., Carey, A., Brickman, J.M., Wynshaw-Boris, A., and Scambler, P.J. (2002). Targeted

mutagenesis of the Hira gene results in gastrulation defects and patterning abnormalities of mesoendodermal derivatives prior to early embryonic lethality. Mol. Cell. Biol. *22*, 2318–2328.

Sakai, A., Schwartz, B.E., Goldstein, S., and Ahmad, K. (2009). Transcriptional and developmental functions of the H3.3 histone variant in Drosophila. Curr. Biol. *19*, 1816–1820.

Saxonov, S., Berg, P., and Brutlag, D.L. (2006). A genome-wide analysis of CpG dinucleotides in the human genome distinguishes two distinct classes of promoters. Proc. Natl. Acad. Sci. USA *103*, 1412–1417.

Schneiderman, J.I., Sakai, A., Goldstein, S., and Ahmad, K. (2009). The XNP remodeler targets dynamic chromatin in Drosophila. Proc. Natl. Acad. Sci. USA *106*, 14472–14477.

Schoeftner, S., and Blasco, M.A. (2008). Developmentally regulated transcription of mammalian telomeres by DNA-dependent RNA polymerase II. Nat. Cell Biol. *10*, 228–236.

Schones, D.E., Cui, K., Cuddapah, S., Roh, T.Y., Barski, A., Wang, Z., Wei, G., and Zhao, K. (2008). Dynamic regulation of nucleosome positioning in the human genome. Cell *132*, 887–898.

Schwartz, B.E., and Ahmad, K. (2005). Transcriptional activation triggers deposition and removal of the histone variant H3.3. Genes Dev. *19*, 804–814.

Sfeir, A., Kosiyatrakul, S.T., Hockemeyer, D., MacRae, S.L., Karlseder, J., Schildkraut, C.L., and de Lange, T. (2009). Mammalian telomeres resemble fragile sites and require TRF1 for efficient replication. Cell *138*, 90–103.

Siegel, T.N., Hekstra, D.R., Kemp, L.E., Figueiredo, L.M., Lowell, J.E., Fenyo, D., Wang, X., Dewell, S., and Cross, G.A. (2009). Four histone variants mark the boundaries of polycistronic transcription units in Trypanosoma brucei. Genes Dev. *23*, 1063–1076.

Smith, S., and Stillman, B. (1989). Purification and characterization of CAF-I, a human cell factor required for chromatin assembly during DNA replication in vitro. Cell *58*, 15–25.

Stock, J.K., Giadrossi, S., Casanova, M., Brookes, E., Vidal, M., Koseki, H., Brockdorff, N., Fisher, A.G., and Pombo, A. (2007). Ring1-mediated ubiquitination of H2A restrains poised RNA polymerase II at bivalent genes in mouse ES cells. Nat. Cell Biol. *9*, 1428–1435.

Sutcliffe, E.L., Parish, I.A., He, Y.Q., Juelich, T., Tierney, M.L., Rangasamy, D., Milburn, P.J., Parish, C.R., Tremethick, D.J., and Rao, S. (2009). Dynamic histone variant exchange accompanies gene induction in T cells. Mol. Cell. Biol. *29*, 1972–1986.

Tagami, H., Ray-Gallet, D., Almouzni, G., and Nakatani, Y. (2004). Histone H3.1 and H3.3 complexes mediate nucleosome assembly pathways dependent or independent of DNA synthesis. Cell *116*, 51–61.

Talbert, P.B., and Henikoff, S. (2009). Chromatin-based transcriptional punctuation. Genes Dev. *23*, 1037–1041.

Tamura, T., Smith, M., Kanno, T., Dasenbrock, H., Nishiyama, A., and Ozato, K. (2009). Inducible deposition of the histone variant H3.3 in interferon-stimulated genes. J. Biol. Chem. *284*, 12217–12225.

Tang, J., Wu, S., Liu, H., Stratt, R., Barak, O.G., Shiekhattar, R., Picketts, D.J., and Yang, X. (2004). A novel transcription regulatory complex containing death domain-associated protein and the ATR-X syndrome protein. J. Biol. Chem. *279*, 20369–20377.

Urnov, F.D., Miller, J.C., Lee, Y.L., Beausejour, C.M., Rock, J.M., Augustus, S., Jamieson, A.C., Porteus, M.H., Gregory, P.D., and Holmes, M.C. (2005). Highly efficient endogenous human gene correction using designed zinc-finger nucleases. Nature *435*, 646–651.

Wang, Z., Zang, C., Rosenfeld, J.A., Schones, D.E., Barski, A., Cuddapah, S., Cui, K., Roh, T.Y., Peng, W., Zhang, M.Q., and Zhao, K. (2008). Combinatorial patterns of histone acetylations and methylations in the human genome. Nat. Genet. *40*, 897–903.

Wong, L.H., Ren, H., Williams, E., McGhie, J., Ahn, S., Sim, M., Tam, A., Earle, E., Anderson, M.A., Mann, J., and Choo, K.H. (2009). Histone H3.3 incorporation provides a unique and functionally essential telomeric chromatin in embryonic stem cells. Genome Res. *19*, 404–414.

Xue, Y., Gibbons, R., Yan, Z., Yang, D., McDowell, T.L., Sechi, S., Qin, J., Zhou, S., Higgs, D., and Wang, W. (2003). The ATRX syndrome protein forms a chromatin-remodeling complex with Daxx and localizes in promyelocytic leukemia nuclear bodies. Proc. Natl. Acad. Sci. USA *100*, 10635–10640.

Note Added in Proof

While this manuscript was in press, Wong et al. reported that Atrx associates with histone H3.3 and localizes to telomeres in mouse ESCs (Wong et al., 2010). These data further support our conclusion that distinct factors control H3.3 localization at specific genomic regions.

Wong, L.H., McGhie, J.D., Sim, M., Anderson, M.A., Ahn, S., Hannan, R.D., George, A.J., Morgan, K.A., Mann, J.R., and Choo, K.H. (2010). ATRX interacts with H3.3 in maintaining telomere structural integrity in pluripotent embryonic stem cells. Genome Res., in press.

EXTENDED EXPERIMENTAL PROCEDURES

Mouse ES Cells

The parental "C6" ES line was derived from tyrosinase −/− (white, albino) homozygous mouse embryos of B6(Cg)-Tyrc-2J/J C57BL/6J background. http://jaxmice.jax.org/strain/000058.html The parental "965" ES line is an F1 hybrid 129SVJae x *M. m. castaneus* (Eggan et al., 2001; Mikkelsen et al., 2007), and was a gift from Rudolf Jaenisch. Hira −/− ES cells, *Atrx*^{flox}, and *Atrx*^{null} ES cells have been described previously (Garrick et al., 2006; Meshorer et al., 2006).

Zinc Finger Nuclease Design and Validation

Zinc finger nucleases (ZFNs) were designed against a region immediately upstream of the H3.3 stop codon (Figure S1B), since gene conversion tracts from DSBs induced by I-SceI (Elliott et al., 1998) and by ZFNs (Figure S1I) in somatic mammalian cells are rather narrow. Our goal was to both tag the native H3.3B ORF at the C terminus (Figures 1C and 1D) as well as co-convert the H3.3B coding region to a H3.2 or H3.1 allelic form (Figures S1C and S1D). We designed ZFNs using an archive of validated two-finger modules (Doyon et al., 2008; Shukla et al., 2009; Urnov et al., 2005). ZFNs were assembled using a PCR-based method, cloned into expression vectors and validated as described (Urnov et al., 2005). The ZFNs used carried obligate heterodimer forms of the FokI endonuclease (Miller et al., 2007). The ZFN target sequences and the recognition helices are provided below.

ZFN target site and designed zinc finger helices sequences were as follows:

Locus: h3f3b
ZFN: #25000
ZFN binding sequence (underlined): CTGTAGGTCAACCGAGCGGCCTATGCCCC
Finger 1: RSDHLSE
Finger 2: RNDTRKT
Finger 3: QSSNLAR
Finger 4: RSDDRKT
Locus: h3f3b
ZFN: #25001
ZFN binding sequence (underlined): GACATCCAGTTGGCTCGCCGGATACGGGG
Finger 1: DRSALSR
Finger 2: TSANLSR
Finger 3: RSDVLSE
Finger 4: QRNHRTT

H3.3B EYFP and HA-IRES-EYFP Donor Plasmid Construction

Briefly, a PCR fragment of genomic DNA from mouse H3.3B was cloned out of a genomic bacterial artificial chromosome (BAC) from C57BL/6J mouse chromosome 11 using Phusion polymerase (NEB F-530L) and into a pCR2.1 vector (pCR2.1-H3.3B) using TA-TOPO cloning (Invitrogen K4500-02). To generate the H3.3B-EYFP donor construct (pCR2.1-H3.3B-EYFP), a 6 amino acid (SRPVAT) linker (Ahmad and Henikoff, 2002) followed by the open-reading frame of EYFP (Clontech) was inserted in-frame into the last coding exon of H3.3B, using ligation-independent cloning (LIC) (Geiser et al., 2001) The H3.3B-EYFP donor included no H3.3B promoter sequence, containing approximately 0.6kb of 5′ homologous genomic sequence starting at the second H3.3B codon, including introns, until the last H3.3B coding amino acid, followed by the linker and EYFP, a stop codon, and approximately 1.3kb homologous to the H3.3B 3′UTR (see Figure S1C). To generate the H3.3B-HA-IRES-EYFP construct (pCR2.1-H3.3B-HA-IRES-EYFP), a C-terminal HA-IRES sequence was cloned out of the vector pMSCV-F-del Casp9.IRES.GFP (Straathof et al., 2005), Addgene Plasmid 15567, and inserted in-frame using LIC into the pCR2.1-H3.3B-EYFP vector. To generate H3.2-EYFP, H3.1-EYFP, H3.2-HA-IRES-EYFP, and H3.1-HA-IRES-EYFP donors, point mutations were made in pCR2.1-H3.3B-EYFP and pCR2.1-H3.3B-HA-IRES-EYFP using the Quick-Change Mutagenesis II kit (Stratagene).

ZFN Targeting and Verification

To deliver ZFNs and donor constructs, mouse ES cells were transfected by Amaxa nucleofection. In brief, immediately prior to transfection, ES cells were feeder depleted by harvesting the ES cells, plating on a feeder-free dish for 30min, and then collecting the ES-enriched non-adherent cells for transfection. 2-5*10$\hat{6}$ cells ES cells were resuspended in 90 μl solution, mixed with two non-linearized plasmids (1 μg of ZFN plasmid with both ZFNs separated by a 2A peptide sequence + 10 μg of donor plasmid) in 10 μl nucleofection solution, and transfected using program A-013 as described in the Amaxa manufacturer's protocol for mouse ES cells. Following transfection, we used sterile plastic pipettes to transfer the cells to warm ES media in tissue culture dishes that were already prepared with feeders. After transfer, ES cells were cultured in standard conditions on treated feeders for 3-5 days prior to fluorescent activated cell sorting (FACS) (Figures S1E and S1F) or fluorescent colony picking. Following colony picking, clonal isolation and expansion, we prepared genomic DNA using the QIAGEN DNeasy Blood & Tissue Kit (QIAGEN 69504). Individual clones were screened by PCR

using a forward H3.3B primer (TTGGTGGAGTATCTGCCCGTTCTG) outside of the donor construct and reverse primer (GTTCTTCTGCTTGTCGGCCATGATA) within EYFP (Figures S1C and S1D and data not shown). To verify that the wild-type H3.3B allele remained intact, we also amplified both H3.3B alleles by using the same forward primer above, and a reverse primer (TGAAGCCAACCTGCTGCTCTACAGT) outside the donor construct, performed gel electrophoresis, and isolated the smaller band corresponding to the wild-type H3.3B allele (data not shown). PCR products from both wild-type and modified H3.3B alleles were sequenced using standard methods (data not shown). To confirm heterozygosity, we used the primers described above to sequence both H3.3B alleles from all ES lines used in this study. For further confirmation of heterozygosity, we performed Southern blotting on a subset of the ES lines. To perform Southern blotting, we digested genomic DNA from wild-type and targeted ES cells with BsrBI, and used a labeled 638bp AvaII fragment of the H3.3B donor as probe to visualize wild-type H3.3B and integrated H3.3B donors (Figure S1G). All targeted C6 ES lines used for manuscript were found to be pure heterozygotes. The hybrid H3.3-HA ES line and the Hira −/− H3.3-EYFP ES lines were heterozygous, with one H3.3B allele targeted, but also had additional donor integrations by Southern blot. Western blot analysis indicates that the hybrid ES H3.3-HA is not overexpressed relative to the pure heterozygote hybrid H3.1S31-HA ES line (data not shown), and global patterns of H3.3 were extremely similar to patterns in the pure heterozygous C6 H3.3-HA and H3.3-EYFP ES lines. H3.3-HA and H3.2-HA ES cells were also fully karyotyped, and found to have normal male mouse karyotypes (data not shown).

ES Cell Culture and NPC Differentiation

For early passages, ES cells were maintained on mitomycin C treated feeders in standard ES cell media, KO-DMEM (Invitrogen 10829-018), 2mM L-glutamine (Sigma G7513) and pen-strep, 15% ES grade fetal bovine serum (GIBCO 10439-024), 10-4 mM 2-mercaptoethanol, and leukemia inhibitory factor (LIF). To remove feeders for ES cell whole cell extracts, chromosome spreads, ChIP, and NPC differentiation, ES cells were passaged at least two passages off of feeders on to gelatin-coated plates. NPC differentiation was performed as described (Conti et al., 2005). We cultured and expanded NPCs on gelatin-coated plates in NeuroCult® NSC Basal Medium (Mouse, Stem Cell Technologies, cat#05700) supplemented with 2mM final L-glutamine and pen-strep (Omega Scientific PG-30), modified N2 supplement freshly prepared in house as described (Conti et al., 2005), and 10ng/ml of both mouse EGF (Peprotech 315-09) and human FGF-2 (Peprotech 100-18B).

RT-PCR

Total RNA from ES cells and NPCs was isolated using TRIzol Reagent (Invitrogen). 1 μg of RNA from each sample was used to generate cDNA using the Superscript First-Strand Synthesis kit (Invitrogen). Real-time PCR was performed with SYBR Green PCR master mix (Applied Biosystems) according to the manufacturer's instructions. Pooled cDNA was used to generate a standard curve from which the relative amount of cDNA amplified in each sample was determined as indicated. Primer sequences for RT-PCR are as follows. *Gapdh*_F: GGTTGTCTCCTGCGACTTCAACAGC, *Gapdh*_R: CGAGTTGGGATAGGGCCTCTCTTGC (Chew et al., 2005), *Pou5f1*_F: TTGGGCTAGAGAAGGATGTGGTT, *Pou5f1*_R: GGAAAAGGGACTGAGTAGAGTGTGG (Chew et al., 2005), *Nanog*_F: CCTCTTCAAGGCAGCCCTGATTCT, *Nanog*_R: AGAGTTCTTGCATCTGCTGGAGGCT, *Olig1*_F: GCTCGCCCAGGTGTTTTGT, *Olig1*_R: GCATGGAACGTGGTTGGAAT (Boyer et al., 2006), *h3f3a*_F: ACAAAAGCCGCTCGCAAGAG, *h3f3a*_R: ATTTCTCGCACCAGACGCTG, *h3f3b*_F: TGGCTCTGAGAGAGATCCGTCGTT, *h3f3b*_R: GGATGTCTTTGGGCATGATGGTGAC.

Flow Cytometry

FACS and analysis was performed on a BD FACSAriaII-2. In brief, ES cells were trypsinized and gently separated to single cells for FACS, and resuspended in PBS + 5% ES quality FBS (GIBCO 10439-024). FACS collection tubes were pre-coated with ES quality FBS for at least 30 min prior to the sort. To prevent clumping during the sort, cells were gently filtered into a single cell suspension through a cell-strainer mesh (Polystyrene Round-Bottom Tube with Cell-Strainer Cap, Falcon #352235). Following sort, cells were immediately plated on feeders with ES media.

Metaphase Chromosome Spreads

Chromosome spreads were performed as described (Perez-Burgos et al., 2004).

Isolation of Protein Complexes and Mass Spectrometric Analysis

Immunoaffinity purications of GFP-tagged H3.3, H3.2, H3.1, H3.3 HIRA−/−, and H3.2 HIRA −/− were performed as previously described (Cristea et al., 2005). Briefly, for each isolation, ~2.5g cryogenically ground cells were extracted in 9 ml of 20 mM K-HEPES, pH 7.4, 110 mM K-acetate, 0.1% Tween 20, 0.5% Triton, 300 mM NaCl, and 1/100 (v/v) protease inhibitor cocktail (Sigma-Aldrich). Resulting cell homogenates were incubated with 12 mg M-270 epoxy magnetic beads (Dynal, Oslo, Norway), conjugated with in-house developed rabbit polyclonal anti-GFP antibodies (5μg antibodies/mg beads) for one hour at 4°C. Isolated proteins were eluted in 700 μl 0.5N NH4OH, 0.5mM EDTA for 20 min at room temperature, dried by vacuum centrifugation, suspended in protein electrophoresis sample buffer, resolved by 1-D SDS-PAGE (4%–12% NuPAGE Novex Bis-Tris gel, Invitrogen), and stained with Coomassie Blue (GelCode Blue, Pierce). The entire gel lanes were cut into sections (~30 sections per gel lane), and proteins were digested with 12.5ng/μl sequencing grade modified trypsin (Promega, WI, USA). Resulting peptides were

extracted on reverse phase resin (Poros 20 R2, PerSeptive Biosystems), eluted in 2 mg/ml α-cyano-4-hydroxycinnamic acid, 70% (v/v) acetonitrile and 0.1% (v/v) trifluoroacetic acid, and deposited onto an in-house made magnetic MALDI target, as described (Blethrow et al., 2007). MALDI MS and MS/MS analyses were performed using prOTOF (Perkin Elmer), vMALDI LTQ XL (Thermo Electron, Bremen, Germany), and MALDI LTQ Orbitrap XL (Thermo) mass spectrometers, as described (Blethrow et al., 2007; Luo et al., 2009). Protein candidates were identified by database searching against the most recent version of the National Center for Biotechnology Information nonredundant protein database using the XProteo computer algorithm (http://www.xproteo.com). The MS/MS CID data was acquired and interpreted manually to confirm the candidate peptides.

Antibodies

Antibodies used for Western blotting, immunofluorescence, and ChIP-seq were as follows. H3K4me1 (Abcam ab8895), H3K4me3 (Abcam ab8580), H3K27me3 (Upstate/Millipore #07-449), H3K36me3 (Abcam ab9050), RNA polymerase CTD phosphorylated on Ser5 CTD4H8 (Upstate/Millipore #05-623), C-terminal H3 (Abcam ab1791), anti-HA (mouse monoclonal 12CA5, western and ChIP-seq), anti-HA (mouse monoclonal HA.11, Covance MMS-101R, immunofluorescence), Oct-3/4 (BD Biosciences 611202), affinity-purified rabbit polyclonal anti-GFP (Cristea et al., 2005), Ldha (Santa Cruz H-160, sc-33781), Atrx (mouse monoclonal 23c) (McDowell et al., 1999). The anti-Nestin hybridoma (Rat-401) developed by Susan Hockfield was obtained from the Developmental Studies Hybridoma bank developed under the auspices of the NICHD and maintained by the University of Iowa, Dept. of Biological Sciences, Iowa City, IA 52242. The mouse monoclonal anti-Hira antibody (WC119) was a gift from Peter D. Adams (Hall et al., 2001).

Crosslinking and Native ChIP

ChIP is generally performed with either formaldehyde-mediated crosslinking of proteins and nucleic acids within living cells followed by sonication (crosslinking, x-link ChIP) or by micrococcal nuclease digestion of harvested cell nuclei and isolation of solubilized mono or short oligonucleosomes (native ChIP). Crosslinking ChIP 'freezes' protein and nucleic acid interactions and enables the analysis of nucleosomal as well as non-nucleosomal proteins such as TFs and RNA polymerase, while native ChIP is more suitable for the analysis of core chromatin and nucleosomal components such as histones and histone modifications (Kuo and Allis, 1999; O'Neill and Turner, 2003). We used a slightly modified version of described protocols (Barski et al., 2007; Lee et al., 2006) to perform both native and crosslinking ChIP. Both protocols use Invitrogen Dynal magnetic beads (Invitrogen Dynabeads anti-mouse M-280 #112-02, or Dynabeads anti-rabbit M-280 #112-04, or Dynabeads Protein A #100-02D). We have found that these magnetic beads generate low background when washed as described (Barski et al., 2007; Lee et al., 2006), and also are free of salmon sperm DNA which might otherwise contaminate ChIP-seq results. For x-link ChIP, we harvested ES cells and NPCs immediately prior to fixation with 1% paraformaldehyde, as we found that crosslinking on gelatin-coated plates also crosslinks gelatin. Approximately 1*10̂7 cells were used for each ChIP. For sonication, we used a Bioruptor (Diagenode) and optimized sonication conditions to generate DNA fragments of approximately 300-500 bp. Following the x-link ChIP protocol (Lee et al., 2006) through overnight crosslink reversal at 65°C, RNase digestion, and proteinase K digestion with modifications as described above, we then isolated ChIP DNA and ChIP input DNA using the QIAGEN Qiaquick PCR purification kit (28104), eluting in 50 μl 10 mM Tris pH 8.5. Atrx ChIP was performed using a modfication of the x-link ChIP protocol (Lee et al., 2006), and is described in detail in Law et al. (manuscript in preparation). For native ChIP, we used the published protocol (Barski et al., 2007) as described, with slight modifications. Following the final wash, we eluted off of magnetic beads using 50mM Tris-HCl pH 8.0, 10 mM EDTA, and 1% SDS, as described in the x-link ChIP protocol (Lee et al., 2006). Following elution, we digested proteins with proteinase K (Roche, recombinant, PCR grade, 03115828001), and isolated DNA with QIAGEN PCR purification kit as described above for x-ChIP. To confirm telomere enrichment, ChIP-seq DNA libraries were also probed with a TTAGGG repeat probe and BamHI repeat probe as described (Sfeir et al., 2009).

Validation of ChIP-Seq

To validate our ChIP-seq results, we used real-time PCR with SYBR Green PCR master mix (Applied Biosystems) to amplify ChIP samples and ChIP inputs, determining % input of ChIP samples at target locations and control intergenic locations. Primer sequences and ES % inputs are listed in Table S1.

ChIP-Seq

For ChIP-seq of x-link or native ChIP DNA, we took 30 ul of remaining ChIP DNA or ~180ng of input DNA, repaired DNA ends to generate blunt-ended DNA using the Epicenter DNA ENDRepair kit (Epicenter Biotechnologies, cat# ER0720), and purified repaired DNA using QIAGEN PCR purification kit (28104). Following DNA END Repair, we added A bases to the 3′ end of the DNA fragments using Klenow Fragment (NEB M0212L), and purified DNA using QIAGEN MinElute (28004). We ligated IIIlumina/Solexa adapters (#FC-102-1003) to DNA fragments overnight, using T4 DNA ligase (NEB M0202L). Following overnight ligation, we purified adaptor-ligated DNA fragments with QIAGEN MinElute. To generate libraries for Solexa sequencing, we performed 18 cycles of PCR with Illumina/Solexa primers 1.1 and 2.1, checked the fragment size for 1/10 of our amplified library on an agarose gel, and purified the remaining ChIP-seq library using QIAGEN MinElute. We did not use gel purification to isolate our library, as standard methods of gel purification have been shown to decrease the representation of A+T-rich sequences (Quail et al., 2008), and we have also found decreased DNA yield following gel purification (data not shown). The purified DNA was used for cluster generation on Illumina/Solexa

flow cells, and sequencing analysis was performed on an Illumina/Solexa Genome Analyzer 2 following manufacturer protocols. Table S3 lists ChIP-seq assays performed and total tag# for each experiment.

Data Analysis

Genome-wide Density Maps of H3 Variants and Determination of Enriched Regions

All reads were mapped to the mouse genome (build 37, or mm9) using the ELAND alignment software within the Illumina Analysis Pipeline in multi/extended mode. Unique reads mapped to a single best-matching location with no more than two mismatches were kept. During our data analysis, each read was extended 100 nt in its 3′ direction to account for the estimated ChIP DNA fragment size of ~300 bp. Using these extensions, we generated genome-wide distributions of H3 variants, histone modifications, and RNAPII represented by the number of reads spanning individual genomic locations. These profiles were displayed in the Affymetrix Integrated Genome Browser (IGB) and also used for the determinations of genomic regions enriched with ChIP-Seq signals. Like H3K36me3, the signals for H3.3 are very dispersed and often found in large extended regions (Figures 2 and 3). As a result, we tried several existing peak identification programs and found that they were not very effective in identification of H3.3 enriched regions. We therefore employed a simple segmentation algorithm. We first applied a Poisson distribution to model the genome-wide ChIP-Seq profile, and then selected positions with read coverage above a threshold that was determined for each experiment specifically at the p-value of 0.1. Adjacent positions above this threshold and less than 600 bp apart were then merged to form genomic blocks, which were subsequently filtered by a minimal length of 300 bp to generate candidates of enriched regions. The final enriched regions, furthermore, must also have twice more reads in a ChIP assay than its control input run (after normalization by read depths). As a comparison, 95% and 97% of the peaks identified by our method for H3K4me1 and H3K4me3 ChIP-Seq experiments, respectively, were also determined as peaks by a popular ChIP-Seq peak analysis program, MACS (Zhang et al., 2008), suggesting that we only called peaks of high confidence. Figure 1B summarizes the numbers of enriched regions for selected ChIP-experiments and their spatial relationships to gene annotation and transcription factor binding sites.

The Relative Enrichment of H3 Variants in Repetitive Elements

Reads were aligned directly to a library of mouse consensus repetitive sequences (http://www.girinst.org). The proportion of reads aligning to each class of repeats was computed for H3.3, H3.2, and H3.1S31, on the condition that the alignment length and sequence identity must be $\geq$ 25-bp and $\geq$ 90%, respectively. The resulting numbers were compared to the corresponding proportions calculated for input controls to yield relative fold-enrichments.

Distributions of H3 Variants in Transcription Start and End Sites

The reference gene (refSeq or known genes) annotation was downloaded from the UCSC browser (http://genome.ucsc.edu), and genes were segregated into low, medium and high expression based on expression data obtained from a previous microarray analysis (Mikkelsen et al., 2007). The expression values for these three categories were defined as 5~20, 50~200, and > 500, respectively. Based on the CpG contents in their promoters, genes were further divided into three types: high (HCP), intermediate (ICP) and low CpG (LCP) promoters (Mikkelsen et al., 2007). Data shown here are mostly for low, medium and high expression HCP genes (~1800 genes in each group). The three groups of genes were comparatively analyzed for density profiles of H3 variants or modifications around their transcription start sites (TSSs) and transcription end sites (TESs). Briefly, after dividing the ± 5kb regions across TSSs (or TESs) into 50 non-overlapping windows (200-bp in size), we summed the number of ChIP-Seq reads ending in each window over all genes. The sums were then normalized by the gene number in each group and the total of mapped reads obtained in a ChIP-Seq experiment to generate final aggregated ChIP-Seq profiles of H3 variants or modifications. This sliding window method was also applied to analyze a set of genes with ''bivalent'' marks at their promoters in mouse ES cells but not in mouse NPC (Mikkelsen et al., 2007).

The Relative Enrichment of H3 Variants in TFBS

The lists of binding sites for 13 transcription factors in mouse ES cells were obtained from a previous ChIP-Seq analysis (Chen et al., 2008). RefSeq gene annotation was used to segregate TFBS into three groups: promoter (±5 kb of TSS), intergenic (5 kb away from genes), and otherwise gene body. After extending each of these TFBS from its 5′ and 3′ direction to span 10-kb sequence, we applied a sliding-window approach, similar to the one for TSSs, to generate density profiles over TFBS for different H3 variants or histone modifications. (Chen et al., 2008) has also defined a set of multiple transcription factor-binding loci (MTL) that were bound by more than four different transcription factors. For these MTL, we computed the read density (number of reads per 5-kb sequence) to characterize the correlation between number of bound factors and the abundance of different H3 variants.

Immuno-FISH and Microscopy

Cells were grown on glass coverslips coated with poly-L-lysine (Sigma). Cells were washed in PBS and fixed in PBS containing 2% para-formaldehyde for 10 min. After two washes in PBS, cells were incubated in PBS containing 0.5% Triton X-100 for 10 min. For denaturing of the samples, cells were incubated in a standard denaturing solution for 2 min at 72 C. After dehydration of the coverslips in increasing concentrations of ethanol (75%–100% ethanol), cells were subjected to hybridization using a PNA TAMRA-TelG telomere (Tam-OO-TTAGGGTTAGGGTTAGGG 3′) custom made from BioSynthesis) probe at a 1:4000 dilution in a standard hybridization buffer (70% formamide, 0.5% blocking reagent (from 10% stock, Roche 11096176001), 10 mM Tris-HCl pH 7.2 in ddH_2O) overnight at RT. After two washes in washing solution (70% formamide, 10 mM Tris-HCl, ph 7.2) and PBS, samples were incubated with blocking solution (1 mg/ml BSA, 3% normal goat serum, 0.1% Triton X-100, 1 mM EDTA ph 8.0 in PBS) for 30 min at RT. Incubation

with primary rabbit anti-GFP antibody (Cristea et al., 2005) was in blocking solution for for 2h at RT. Secondary anti-rabbit AlexaFluor 488 antibody (Molecular Probes, Invitrogen A21206) was used at 1:1000. Slides were counterstained with TO-PRO-3 iodide (Invitrogen) for 5 min and mounted in ProLong Gold antifade reagent (Invitrogen). Stainings were analyzed using an upright Zeiss LSM 510 confocal laser scanning microscope. Images were obtained using the Zeiss LSM software, and Photoshop CS4 was used to prepare figures.

SUPPLEMENTAL REFERENCES

Ahmad, K., and Henikoff, S. (2002). The histone variant H3.3 marks active chromatin by replication-independent nucleosome assembly. Mol. Cell *9*, 1191–1200.

Barski, A., Cuddapah, S., Cui, K., Roh, T.Y., Schones, D.E., Wang, Z., Wei, G., Chepelev, I., and Zhao, K. (2007). High-resolution profiling of histone methylations in the human genome. Cell *129*, 823–837.

Blethrow, J.D., Tang, C., Deng, C., and Krutchinsky, A.N. (2007). Modular mass spectrometric tool for analysis of composition and phosphorylation of protein complexes. PLoS ONE *2*, e358.

Boyer, L.A., Plath, K., Zeitlinger, J., Brambrink, T., Medeiros, L.A., Lee, T.I., Levine, S.S., Wernig, M., Tajonar, A., Ray, M.K., et al. (2006). Polycomb complexes repress developmental regulators in murine embryonic stem cells. Nature *441*, 349–353.

Chen, X., Xu, H., Yuan, P., Fang, F., Huss, M., Vega, V.B., Wong, E., Orlov, Y.L., Zhang, W., Jiang, J., et al. (2008). Integration of external signaling pathways with the core transcriptional network in embryonic stem cells. Cell *133*, 1106–1117.

Chew, J.L., Loh, Y.H., Zhang, W., Chen, X., Tam, W.L., Yeap, L.S., Li, P., Ang, Y.S., Lim, B., Robson, P., and Ng, H.H. (2005). Reciprocal transcriptional regulation of Pou5f1 and Sox2 via the Oct4/Sox2 complex in embryonic stem cells. Mol. Cell. Biol. *25*, 6031–6046.

Conti, L., Pollard, S.M., Gorba, T., Reitano, E., Toselli, M., Biella, G., Sun, Y., Sanzone, S., Ying, Q.L., Cattaneo, E., and Smith, A. (2005). Niche-independent symmetrical self-renewal of a mammalian tissue stem cell. PLoS Biol. *3*, e283.

Cristea, I.M., Williams, R., Chait, B.T., and Rout, M.P. (2005). Fluorescent proteins as proteomic probes. Mol. Cell. Proteomics *4*, 1933–1941.

Doyon, Y., McCammon, J.M., Miller, J.C., Faraji, F., Ngo, C., Katibah, G.E., Amora, R., Hocking, T.D., Zhang, L., Rebar, E.J., et al. (2008). Heritable targeted gene disruption in zebrafish using designed zinc-finger nucleases. Nat. Biotechnol. *26*, 702–708.

Eggan, K., Akutsu, H., Loring, J., Jackson-Grusby, L., Klemm, M., Rideout, W.M., 3rd, Yanagimachi, R., and Jaenisch, R. (2001). Hybrid vigor, fetal overgrowth, and viability of mice derived by nuclear cloning and tetraploid embryo complementation. Proc. Natl. Acad. Sci. USA *98*, 6209–6214.

Elliott, B., Richardson, C., Winderbaum, J., Nickoloff, J.A., and Jasin, M. (1998). Gene conversion tracts from double-strand break repair in mammalian cells. Mol. Cell. Biol. *18*, 93–101.

Garrick, D., Sharpe, J.A., Arkell, R., Dobbie, L., Smith, A.J., Wood, W.G., Higgs, D.R., and Gibbons, R.J. (2006). Loss of Atrx affects trophoblast development and the pattern of X-inactivation in extraembryonic tissues. PLoS Genet. *2*, e58.

Gaspar-Maia, A., Alajem, A., Polesso, F., Sridharan, R., Mason, M.J., Heidersbach, A., Ramalho-Santos, J., McManus, M.T., Plath, K., Meshorer, E., and Ramalho-Santos, M. (2009). Chd1 regulates open chromatin and pluripotency of embryonic stem cells. Nature *460*, 863–868.

Geiser, M., Cèbe, R., Drewello, D., and Schmitz, R. (2001). Integration of PCR fragments at any specific site within cloning vectors without the use of restriction enzymes and DNA ligase. Biotechniques *31*, 88–90, 92.

Hall, C., Nelson, D.M., Ye, X., Baker, K., DeCaprio, J.A., Seeholzer, S., Lipinski, M., and Adams, P.D. (2001). HIRA, the human homologue of yeast Hir1p and Hir2p, is a novel cyclin-cdk2 substrate whose expression blocks S-phase progression. Mol. Cell. Biol. *21*, 1854–1865.

Huang, W., Sherman, B.T., and Lempicki, R.A. (2009). Systematic and integrative analysis of large gene lists using DAVID bioinformatics resources. Nat. Protoc. *4*, 44–57.

Jin, C., Zang, C., Wei, G., Cui, K., Peng, W., Zhao, K., and Felsenfeld, G. (2009). H3.3/H2A.Z double variant-containing nucleosomes mark 'nucleosome-free regions' of active promoters and other regulatory regions. Nat. Genet. *41*, 941–945.

Kalkum, M., Lyon, G.J., and Chait, B.T. (2003). Detection of secreted peptides by using hypothesis-driven multistage mass spectrometry. Proc. Natl. Acad. Sci. USA *100*, 2795–2800.

Konev, A.Y., Tribus, M., Park, S.Y., Podhraski, V., Lim, C.Y., Emelyanov, A.V., Vershilova, E., Pirrotta, V., Kadonaga, J.T., Lusser, A., and Fyodorov, D.V. (2007). CHD1 motor protein is required for deposition of histone variant H3.3 into chromatin in vivo. Science *317*, 1087–1090.

Kuo, M.H., and Allis, C.D. (1999). In vivo cross-linking and immunoprecipitation for studying dynamic Protein:DNA associations in a chromatin environment. Methods *19*, 425–433.

Lee, T.I., Johnstone, S.E., and Young, R.A. (2006). Chromatin immunoprecipitation and microarray-based analysis of protein location. Nat. Protoc. *1*, 729–748.

Luo, Y., Li, T., Yu, F., Kramer, T., and Cristea, I.M. (2009). Resolving the composition of protein complexes using a MALDI LTQ Orbitrap. J. Am. Soc. Mass Spectrom. *21*, 34–46.

McDowell, T.L., Gibbons, R.J., Sutherland, H., O'Rourke, D.M., Bickmore, W.A., Pombo, A., Turley, H., Gatter, K., Picketts, D.J., Buckle, V.J., et al. (1999). Localization of a putative transcriptional regulator (ATRX) at pericentromeric heterochromatin and the short arms of acrocentric chromosomes. Proc. Natl. Acad. Sci. USA *96*, 13983–13988.

Meshorer, E., Yellajoshula, D., George, E., Scambler, P.J., Brown, D.T., and Misteli, T. (2006). Hyperdynamic plasticity of chromatin proteins in pluripotent embryonic stem cells. Dev. Cell *10*, 105–116.

Mikkelsen, T.S., Ku, M., Jaffe, D.B., Issac, B., Lieberman, E., Giannoukos, G., Alvarez, P., Brockman, W., Kim, T.K., Koche, R.P., et al. (2007). Genome-wide maps of chromatin state in pluripotent and lineage-committed cells. Nature *448*, 553–560.

Miller, J.C., Holmes, M.C., Wang, J., Guschin, D.Y., Lee, Y.L., Rupniewski, I., Beausejour, C.M., Waite, A.J., Wang, N.S., Kim, K.A., et al. (2007). An improved zinc-finger nuclease architecture for highly specific genome editing. Nat. Biotechnol. *25*, 778–785.

O'Neill, L.P., and Turner, B.M. (2003). Immunoprecipitation of native chromatin: NChIP. Methods *31*, 76–82.

Perez-Burgos, L., Peters, A.H., Opravil, S., Kauer, M., Mechtler, K., and Jenuwein, T. (2004). Generation and characterization of methyl-lysine histone antibodies. Methods Enzymol. *376*, 234–254.

Quail, M.A., Kozarewa, I., Smith, F., Scally, A., Stephens, P.J., Durbin, R., Swerdlow, H., and Turner, D.J. (2008). A large genome center's improvements to the Illumina sequencing system. Nat. Methods *5*, 1005–1010.

Sfeir, A., Kosiyatrakul, S.T., Hockemeyer, D., MacRae, S.L., Karlseder, J., Schildkraut, C.L., and de Lange, T. (2009). Mammalian telomeres resemble fragile sites and require TRF1 for efficient replication. Cell *138*, 90–103.

Shukla, V.K., Doyon, Y., Miller, J.C., DeKelver, R.C., Moehle, E.A., Worden, S.E., Mitchell, J.C., Arnold, N.L., Gopalan, S., Meng, X., et al. (2009). Precise genome modification in the crop species *Zea mays* using zinc-finger nucleases. Nature *459*, 437–441.

Straathof, K.C., Pulè, M.A., Yotnda, P., Dotti, G., Vanin, E.F., Brenner, M.K., Heslop, H.E., Spencer, D.M., and Rooney, C.M. (2005). An inducible caspase 9 safety switch for T-cell therapy. Blood *105*, 4247–4254.

Urnov, F.D., Miller, J.C., Lee, Y.L., Beausejour, C.M., Rock, J.M., Augustus, S., Jamieson, A.C., Porteus, M.H., Gregory, P.D., and Holmes, M.C. (2005). Highly efficient endogenous human gene correction using designed zinc-finger nucleases. Nature *435*, 646–651.

Zhang, W., and Chait, B.T. (2000). ProFound: an expert system for protein identification using mass spectrometric peptide mapping information. Anal. Chem. *72*, 2482–2489.

Zhang, Y., Liu, T., Meyer, C.A., Eeckhoute, J., Johnson, D.S., Bernstein, B.E., Nussbaum, C., Myers, R.M., Brown, M., Li, W., and Liu, X.S. (2008). Model-based analysis of ChIP-Seq (MACS). Genome Biol. *9*, R137.

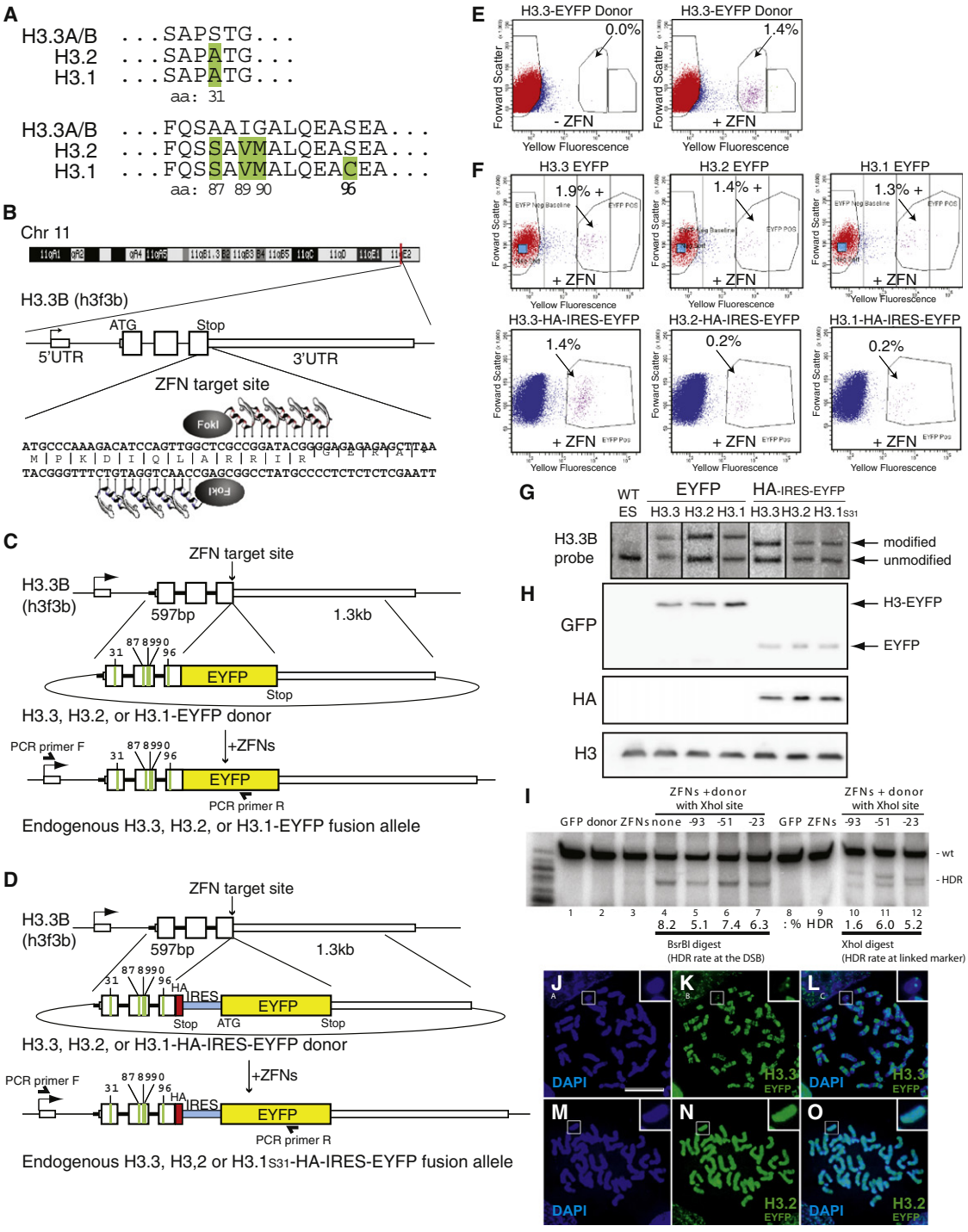

Figure S1. Zinc Finger Nucleases Enable Rapid Knock-in of Epitope Tags and Mutagenesis at Histone H3.3B, Related to Figure 1

(A) Alignment of amino acid sequences for H3 variants H3.3, H3.2, and H3.1. H3.3 differs from H3.2 or H3.1 at only 4 or 5 amino acids, positions 31, 87, 89, 90, and 96.

(B) Zinc finger nucleases (ZFNs) recognize endogenous H3.3B (h3f3b) sequence. Exon sequences are thick rectangles, while non-coding untranslated sequences are thin rectangles.

(C and D) ZFNs target double-strand break (DSB) formation at H3.3B, with H3.3B-EYFP or H3.3B-HA-IRES-EYFP donors generating a new H3.3B allele with a C-terminal EYFP tag (C), or a C-terminal HA tag (red) and an internal ribosomal entry site (IRES, blue) followed by an EYFP reporter (D). ZFN-mediated co-conversion was used to create specific point mutations at positions 31, 87, 89, 90, and 96 (green), generating new H3.3B alleles with C-terminal EYFP or HA-IRES-EYFP sequences and simultaneously converting H3.3 to H3.2, H3.1, or H3.1S31. Location is indicated for primers used for PCR amplification and sequencing (not shown) of modified H3.3B alleles.

(E) Mouse ES cells were transfected with H3.3-EYFP donor alone (left) or H3.3-EYFP donor + ZFNs (right) and analyzed by flow cytometry 3 days post-transfection. Percentage EYFP positive indicated.

(F) Introduction of point mutations decreases efficiency of targeting for H3-EYFP donors (top row) and H3-HA-IRES-EYFP donors (bottom row).

(G) Genomic DNA from wild-type and targeted ES cells was digested with BsrBI and analyzed by Southern blot, using a 638bp AvaII fragment of the H3.3B donor as probe.

(H) Whole cell extracts from wild-type ES and targeted ES cell lines were immunoblotted with GFP, HA, and C-terminal (untagged) H3 antibodies.

(I) Point mutations in donor sequence affect frequency of ZFN-mediated gene correction as well as frequency of adjacent marker co-conversion. A panel of plasmid donors was engineered to carry a novel restriction fragment length polymorphism (RFLP) (BsrBI) at the position of the ZFN-induced DSB in exon 5 of the human IL2Rγ gene, and one additional RFLP (XhoI) at progressively greater distances (23, 51, and 93 bp, respectively) from the DSB site. Only one additional donor per RFLP was engineered. This donor panel was transfected along with the ZFNs into K562 cells, and gene correction frequency at the break (lanes 1-7), as well as marker co-conversion frequency (lanes 8-12) was measured using body-labeled limited-cycle PCR exactly as described (Urnov et al., 2005). The position of wild-type and homology directed repair (HDR) corrected chromatids is indicated to the side of the gel; the frequencies of HDR-carrying chromatids in all cases is shown below each lane.

(J–O) Representative metaphase chromosome spreads from heterozygous H3.3-EYFP / H3.3B and H3.2-EYFP / H3.3B ES cells. ES cells were treated with 0.2 μg/mL colchicine for 2 hr at 37°C. Samples were prepared by cytospin, fixed, stained with DAPI, and visualized using DeltaVision deconvolution microscopy. EYFP and DAPI overlays of maximum-intensity projections from multiple Z-stacks are shown. Bar: 10 μm. Inset shows a higher magnification image of the Y chromosome.

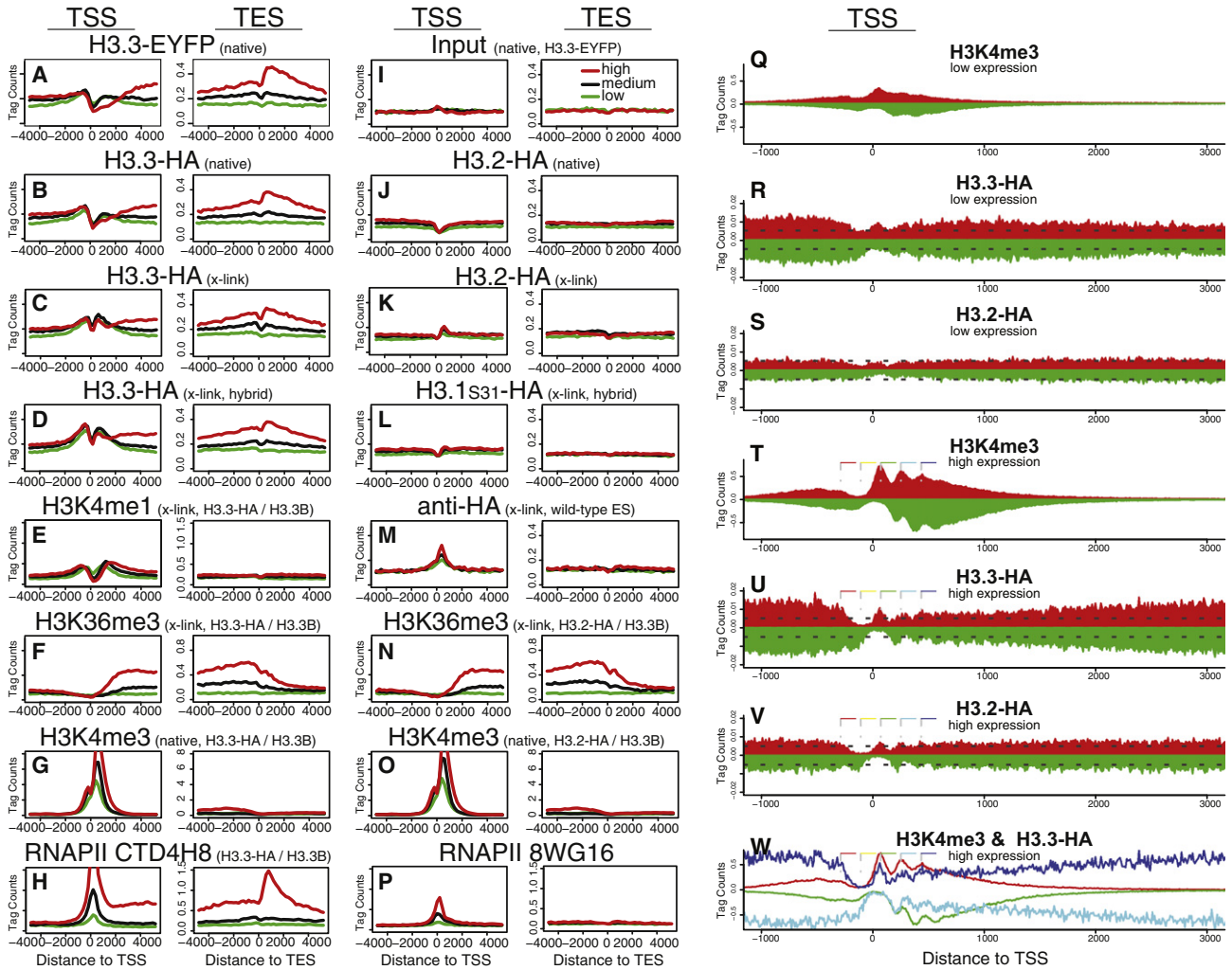
TSS
TES
H3.3-EYFP (native)
A
Input (native, H3.3-EYFP)
I
high
medium
low
H3.3-HA (native)
B
H3.2-HA (native)
J
H3.3-HA (x-link)
C
H3.2-HA (x-link)
K
H3.3-HA (x-link, hybrid)
D
H3.1S31-HA (x-link, hybrid)
L
H3K4me1 (x-link, H3.3-HA / H3.3B)
E
anti-HA (x-link, wild-type ES)
M
H3K36me3 (x-link, H3.3-HA / H3.3B)
F
H3K36me3 (x-link, H3.2-HA / H3.3B)
N
H3K4me3 (native, H3.3-HA / H3.3B)
G
H3K4me3 (native, H3.2-HA / H3.3B)
O
RNAPII CTD4H8 (H3.3-HA / H3.3B)
H
RNAPII 8WG16
P
Tag Counts
Distance to TSS
Distance to TES
TSS
Q
H3K4me3
low expression
R
H3.3-HA
low expression
S
H3.2-HA
low expression
T
H3K4me3
high expression
U
H3.3-HA
high expression
V
H3.2-HA
high expression
W
H3K4me3 & H3.3-HA
high expression
Distance to TSS

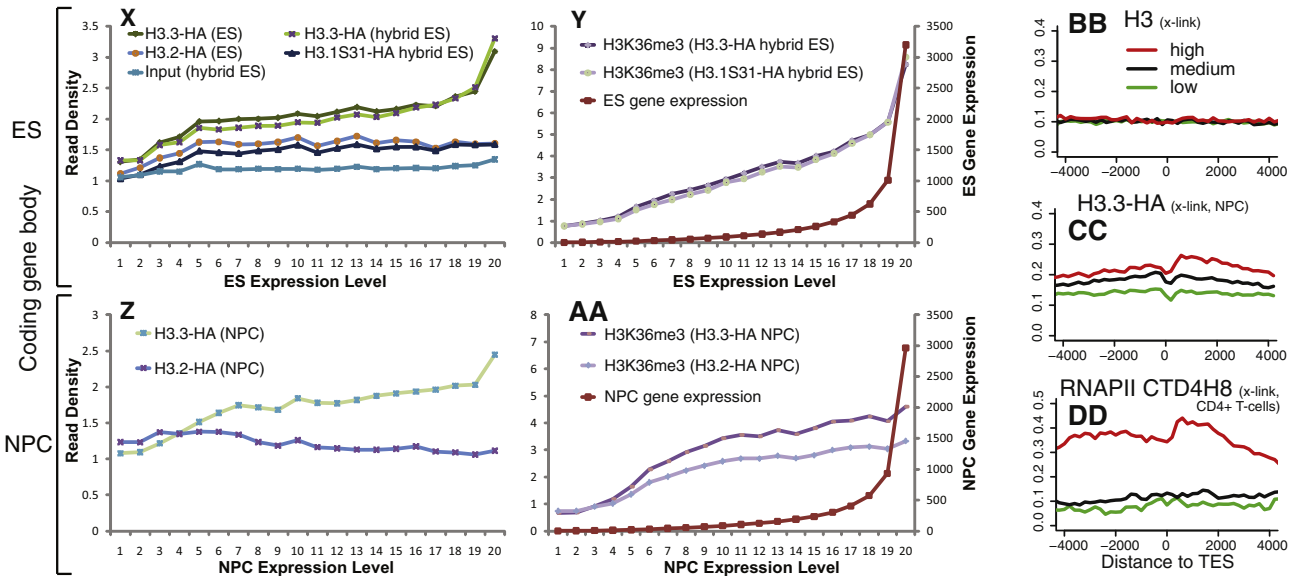
ES
Coding gene body
NPC
X
H3.3-HA (ES)
H3.2-HA (ES)
Input (hybrid ES)
H3.3-HA (hybrid ES)
H3.1S31-HA hybrid ES)
Read Density
ES Expression Level
Y
H3K36me3 (H3.3-HA hybrid ES)
H3K36me3 (H3.1S31-HA hybrid ES)
ES gene expression
ES Gene Expression
Z
H3.3-HA (NPC)
H3.2-HA (NPC)
NPC Expression Level
AA
H3K36me3 (H3.3-HA NPC)
H3K36me3 (H3.2-HA NPC)
NPC gene expression
NPC Gene Expression
BB
H3 (x-link)
high
medium
low
CC
H3.3-HA (x-link, NPC)
DD
RNAPII CTD4H8 (x-link, CD4+ T-cells)
Distance to TES

Figure S2. Genic Patterns and Gene Expression Correlation of H3 Variants and Histone Modifications, Related to Figure 2

(A–P) Profiles of H3 variants, H3 modifications, or controls as indicated above each panel across the transcription start site (TSS) and transcription end site (TES) for highly active, medium expressing, or low expressing CpG rich genes as shown. *y* axis represents the average number of tags per gene per 200 bp per 1 million mapped reads.

(A–D) H3.3 profiles are similar across the TSS and TES for both HA and EYFP-tagged H3.3.

(E) H3K4me1 patterns are similar to H3.3 around the TSS, though levels of H3K4me1 decline into the gene body of highly expressed genes, while H3.3 levels increase and peak beyond the TES.

(F, G, N, and O) Profiles of H3K4me3 and H3K36me3 in H3.3-HA and H3.2-HA ES cells. Heterozygous mutation of H3.3 to H3.2 does not alter genome-wide profiles of H3K4me3 or H3K36me3 around TSS and TES.

(H) Profiles of RNAPII Ser5p in H3.3-HA ES cells at TSS and TES.

(J–L) Mutation of H3.3B toward H3.2 or H3.1 abolishes H3.3 patterns of enrichment.

(M) Background of anti-HA antibody. Sequencing of anti-HA ChIP from untagged wild-type ES cells shows enrichment at the TSS, likely representing the enrichment of nucleosome-poor DNA following cross-linking and sonication.

(P) Profiles of unphosphorylated RNAPII at TSS and TES in ES cells from (Mikkelsen et al., 2007).

(Q–W) Mononucleosome resolution profiles of H3 variants and H3K4me3 at TSS. *y* axis represents average number of tags per gene per 10 bp per million mapped reads. Red represents sense sequence tags, and green represents antisense sequence tags. The color bars (T-V) mark the estimated nucleosomes around TSSs. Data for H3.3 in panel W (dark blue = sense H3.3, light blue = antisense H3.3, red = sense H3K4me3, green = antisense H3K4me3) are scaled by a factor of 50 to match the profile of H3K4me3.

(X–AA) Densities of H3.3 and H3K36me3 reads in coding gene bodies are correlated with gene expression, particularly for highly expressed genes, in both ES (X-Y) and NPC (Z-AA). The left *y* axis represents read density that was computed as average number of ChIP-Seq reads per 2-kb genomic sequence per million mapped reads. Gene expression data are from (Mikkelsen et al., 2007) and the values were uniformly divided into 20 groups to yield genes with low to high levels of expression, with mean gene expression values shown on the right *y* axis in Y and AA. H3.3 deposition in gene bodies is correlated with gene expression, particularly at highly expressed genes (Spearman's rank correlation coefficient $\rho = 0.54$, $p < 2.2e\text{-}16$). By comparison, H3K36me3 shows a greater correlation ($\rho = 0.76$), but H3.1S31 ($\rho = 0.31$) and H3.2 ($\rho = 0.25$) show significantly smaller correlations.

(BB–DD) TES profiles with data represented as in S2A-P. Panel BB is from a previous study in mouse ES cells (Mikkelsen et al., 2007), while panel CC shows data from differentiated NPCs. The data in panel DD are for human CD4+ T cells (Barski et al., 2007).

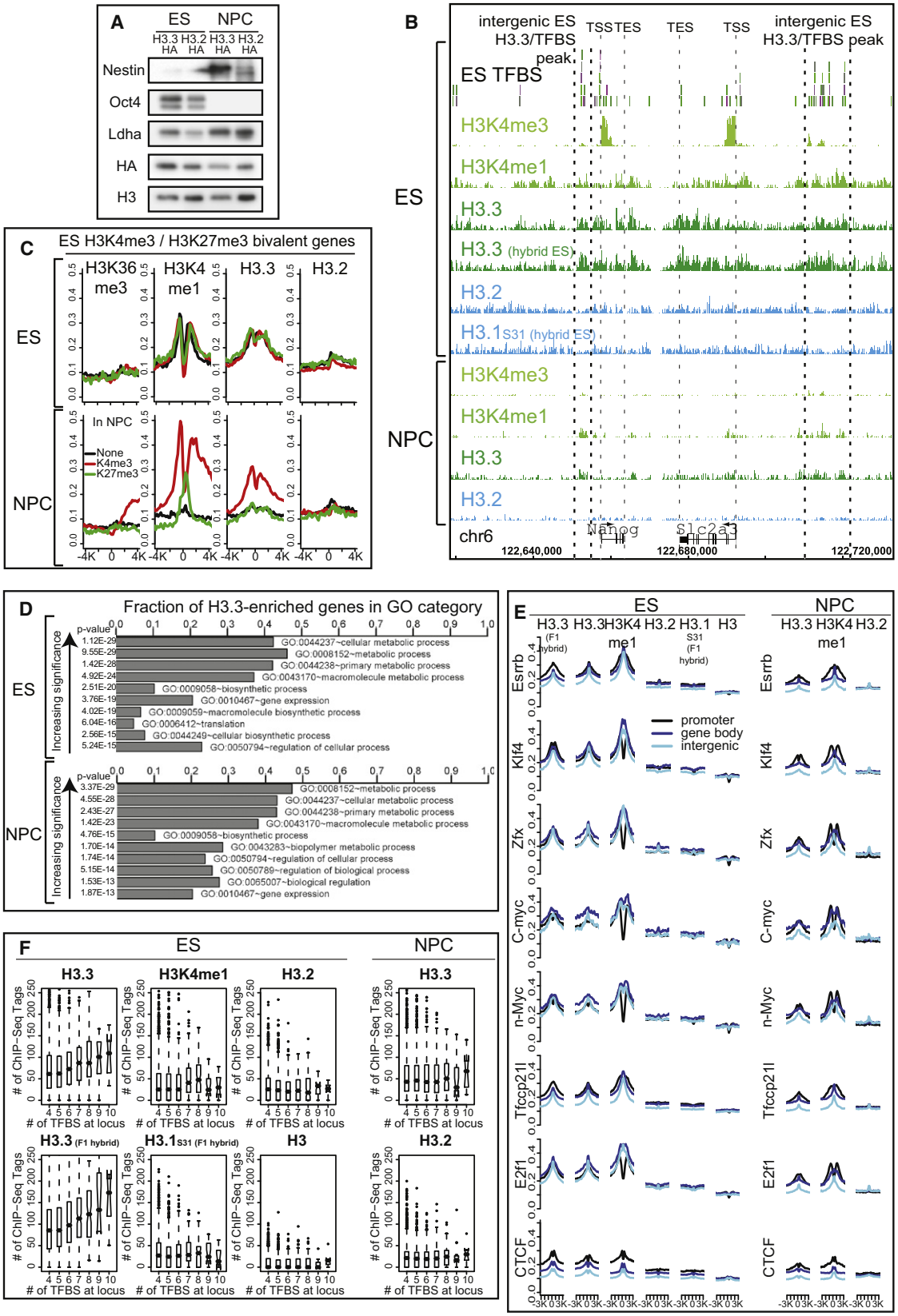
A
ES
NPC
H3.3 HA
H3.2 HA
H3.3 HA
H3.2 HA
Nestin
Oct4
Ldha
HA
H3
B
intergenic ES H3.3/TFBS peak
TSS
TES
TES
TSS
intergenic ES H3.3/TFBS peak
ES TFBS
H3K4me3
H3K4me1
H3.3
H3.3 (hybrid ES)
H3.2
H3.1S31 (hybrid ES)
ES
NPC
H3K4me3
H3K4me1
H3.3
H3.2
chr6
Nanog
S1c2a3
122,640,000
122,680,000
122,720,000
C
ES H3K4me3 / H3K27me3 bivalent genes
H3K36 me3
H3K4 me1
H3.3
H3.2
ES
NPC
In NPC
None
K4me3
K27me3
-4K
0
4K
D
Fraction of H3.3-enriched genes in GO category
ES
NPC
p-value
Increasing significance
1.12E-29 GO:0044237~cellular metabolic process
9.55E-29 GO:0008152~metabolic process
1.42E-28 GO:0044238~primary metabolic process
4.92E-24 GO:0043170~macromolecule metabolic process
2.51E-20 GO:0009058~biosynthetic process
3.76E-19 GO:0010467~gene expression
4.02E-19 GO:0009059~macromolecule biosynthetic process
6.04E-16 GO:0006412~translation
2.56E-15 GO:0044249~cellular biosynthetic process
5.24E-15 GO:0050794~regulation of cellular process
3.37E-29 GO:0008152~metabolic process
4.55E-28 GO:0044237~cellular metabolic process
2.43E-27 GO:0044238~primary metabolic process
1.42E-23 GO:0043170~macromolecule metabolic process
4.76E-15 GO:0009058~biosynthetic process
1.70E-14 GO:0043283~biopolymer metabolic process
1.74E-14 GO:0050794~regulation of cellular process
5.15E-14 GO:0050789~regulation of biological process
1.53E-13 GO:0065007~biological regulation
1.87E-13 GO:0010467~gene expression
E
ES
NPC
H3.3
H3.3 (F1 hybrid)
H3K4 me1
H3.2
H3.1 S31 (F1 hybrid)
H3
H3.3
H3K4 me1
H3.2
promoter
gene body
intergenic
Esrrb
Klf4
Zfx
C-myc
n-Myc
Tfcp2l1
E2f1
CTCF
F
ES
NPC
H3.3
H3K4me1
H3.2
H3.3
H3.3 (F1 hybrid)
H3.1S31 (F1 hybrid)
H3
H3.2
# of ChIP-Seq Tags
# of TFBS at locus

Figure S3. H3.3 Localization in Embryonic Stem Cells and Neuronal Precursor Cells, Related to Figure 3

(A) Whole cell extracts of H3.3-HA and H3.2-HA ES cells and NPCs were immunoblotted with antibodies as indicated.

(B) H3.3 and H3K4me1 are enriched around intergenic and genic TFBS near the *Nanog* gene in ES cells. H3.3-specific enrichment is lost upon mutation of H3.3B to H3.2 or H3.1S31.

(C) Genome-wide profiles of H3.3 at transcription start sites change with cellular differentiation and resolution of bivalent domains. Profiles of H3 variants or H3 modifications as indicated above each panel around the TSS of H3K4me3/H3K27me3 bivalent genes in ES cells. ES bivalent genes are classified by resolution in NPCs to H3K4me3 only (red), H3K27me3 only (green), or no mark (black). H3K4me3/H3K27me3 data and bivalent gene definitions are from (Mikkelsen et al., 2007). Y-axes are as in Figures S2A–S2P.

(D) H3.3 is enriched at genes involved in cellular and metabolic processes in both ES cells and NPC cells. Genes with H3.3 peaks in their promoter regions were analyzed for enrichment of individual GO terms using the program DAVID (Huang da et al., 2009). The top 10 GO categories are shown here with p-values indicated, and the *x* axis representing the fraction of H3.3 genes in a GO category.

(E) H3.3 and H3K4me1 are enriched genome-wide around ES cell TFBS for known ES cell transcription factors Esrrb, Klf4, Zfx, C-myc, n-Myc, Tcfp21l, E2f1, and CTCF. H3.3 enrichment at TFBS is abolished by mutation of H3.3B to H3.2 or H3.1S31, and partially lost upon differentiation of ES cell to NPCs. Data are shown for crosslinking ChIP-seq, using HA-tagged H3.3 and H3.2 ES cells and NPCs. TFBS in mouse ES cells were taken from a previous study (Chen et al., 2008), and classified as promoter, gene body, or intergenic as described in Extended Experimental Procedures. *y* axis represents number of tags per TFBS per 200bp per 1 million mapped reads.

(F) In ES cells and NPCs, levels of H3.3 at ES MTL (Chen et al., 2008) are dependent on H3 amino acid sequence and cellular state. Box-and-whisker plots showing the ChIP-Seq read densities at MTL separated by # of TFBS at a locus (*x* axis). *y* axis represents # of normalized ChIP-Seq tags at a group of MTL with the same # of TFBS, where the central bar is median, box shows 25th and 75th percentiles, and whiskers mark the 1.5x interquartile range.

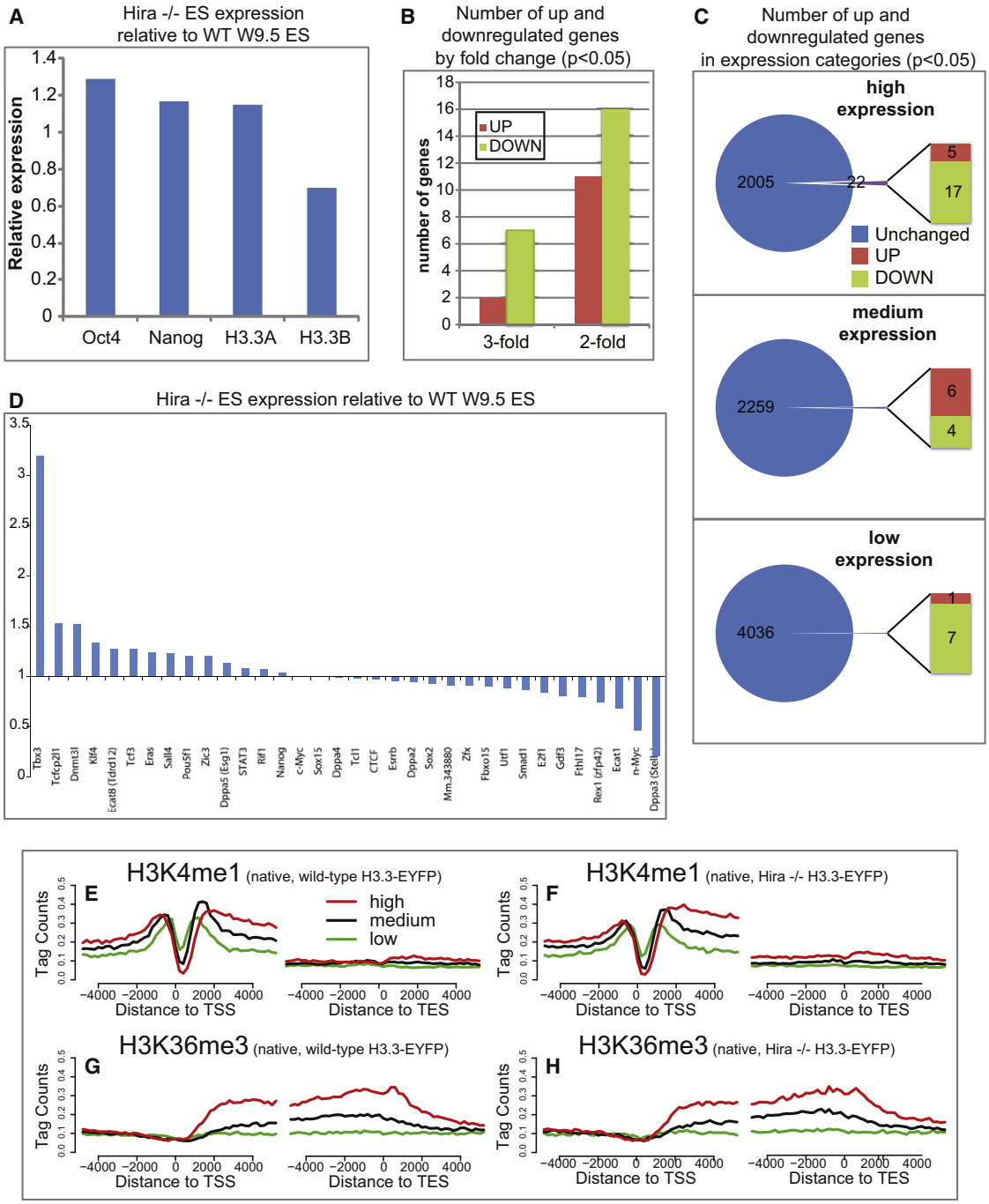

Figure S4. Global Gene Expression and Genic Localization of H3K4me1 and H3K36me3 in Wild-Type and Hira −/− ES Cells, Related to Figure 4

(A) Hira −/− ES cells maintain expression of Oct4, Nanog, H3.3A, and H3.3B. Real-time PCR was performed following RNA extraction and cDNA synthesis. Data were normalized to Gapdh, and plotted as expression in Hira −/− relative to W9.5 ES cells.

(B–D) Triplicate GeneChip® Mouse Gene 1.0 ST Arrays were hybridized with cDNA from three independent biological replicates of HIRA−/− ES (cl34) and WT ES (W9.5) cell lines. The data was analyzed using the LIMMA package of Bioconductor v2.0 and R v.2.9.2, applying GC-RMA normalization and correction for multiple testing (Benjamini-Hochberg) with a significance threshold of $p < 0.05$. B) Significant differentially expressed genes were binned according to their fold-change.

(C) The number of differentially expressed genes was determined for each low, medium, high expression gene sets derived from WT ES cells. High, medium, and low expression genes were determined from a previous microarray of WT ES cells (Mikkelsen et al., 2007) as detailed in Extended Experimental Procedures. Overall, only a small number of genes in these gene sets were affected in Hira −/− ES cells.

(D) Differential expression of ES cell related genes (not corrected for multiple testing).
(E–H) H3K4me1 and H3K36me3 are maintained at TSS in presence and absence of Hira. Profiles of H3K4me1 (E-F) and H3K36me3 (G-H) in wild-type (E,G) and Hira −/− (F,H) H3.3-EYFP ES cells across TSS and TES for highly active, medium, or low expressed CpG rich genes. *y* axis represents the average number of tags per gene per 200 bp per 1 million mapped reads.

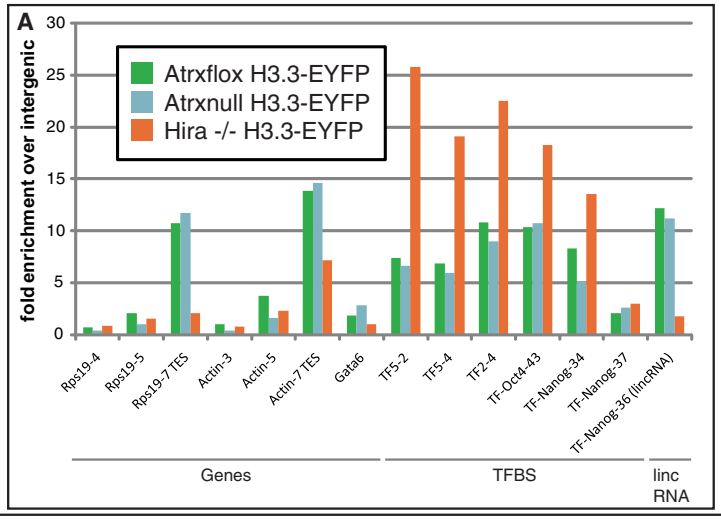
A
fold enrichment over intergenic
30
25
20
15
10
5
0
Atrxflox H3.3-EYFP
Atrxnull H3.3-EYFP
Hira -/- H3.3-EYFP
Rps19-4
Rps19-5
Rps19-7 TES
Actin-3
Actin-5
Actin-7 TES
Gata6
TF5-2
TF5-4
TF2-4
TF-Oct4-43
TF-Nanog-34
TF-Nanog-37
TF-Nanog-36 (lincRNA)
Genes
TFBS
linc RNA

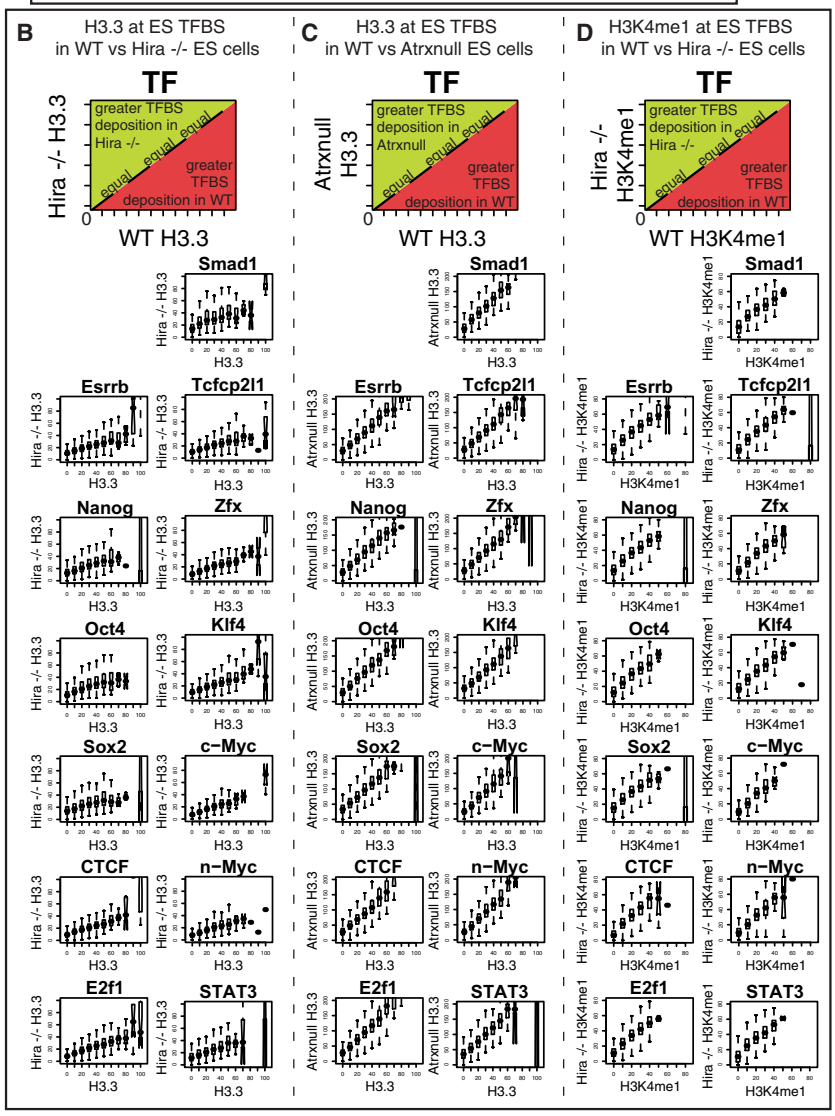
B
H3.3 at ES TFBS in WT vs Hira -/- ES cells
C
H3.3 at ES TFBS in WT vs Atrxnull ES cells
D
H3K4me1 at ES TFBS in WT vs Hira -/- ES cells
TF
Hira -/- H3.3
Atrxnull H3.3
Hira -/- H3K4me1
greater TFBS deposition in Hira -/-
greater TFBS deposition in Atrxnull
greater TFBS deposition in WT
equal
WT H3.3
WT H3K4me1
Smad1
Esrrb
Tcfcp2l1
Nanog
Zfx
Oct4
Klf4
Sox2
c-Myc
CTCF
n-Myc
E2f1
STAT3

Figure S5. H3.3 Enrichment at TFBS Is Not Affected in Atrxnull but Is Partially Perturbed in Hira −/− ES Cells, Related to Figure 5

(A) Real-time PCR of ChIP DNA confirms ChIP-seq results. Note similar profiles of H3.3 at genes and TFBS in Atrxflox (green) and Atrxnull (blue) ES cells. At genes, particularly active gene bodies and TES, H3.3 enrichment is decreased in Hira −/− ES cells (orange), while at TFBS, H3.3 enrichment is Hira-independent. Primer sequences are listed in Table S1. Data are plotted as fold enrichment over intergenic (%input at location / %input at intergenic).

(B) H3.3 read densities at TFBS (Chen et al., 2008) are analyzed and plotted for anti-GFP ChIP-seq experiments from wild-type H3.3-EYFP, Hira −/− H3.3-EYFP, and Atrxnull H3.3-EYFP, and for H3K4me1 ChIP-seq experiments in wild-type and Hira −/− ES cells. TFBS were first separated into different groups based on their H3.3 (or H3K4me1) ChIP-Seq read densities in wild-type (*x* axis) and then their corresponding ChIP-Seq read densities from Hira −/− or Atrx null samples were summarized in *y* axis as boxplots. Note the high correlation of H3K4me1 between wild-type and Hira −/−, and correlation of H3.3 between wild-type and Atrxnull (right two sub-panels). In comparison, H3.3 levels between wild-type and Hira −/− are overall correlated but reduced (left sub-panels), suggesting that Hira affect H3.3 deposition in some but not the majority of TFBS.

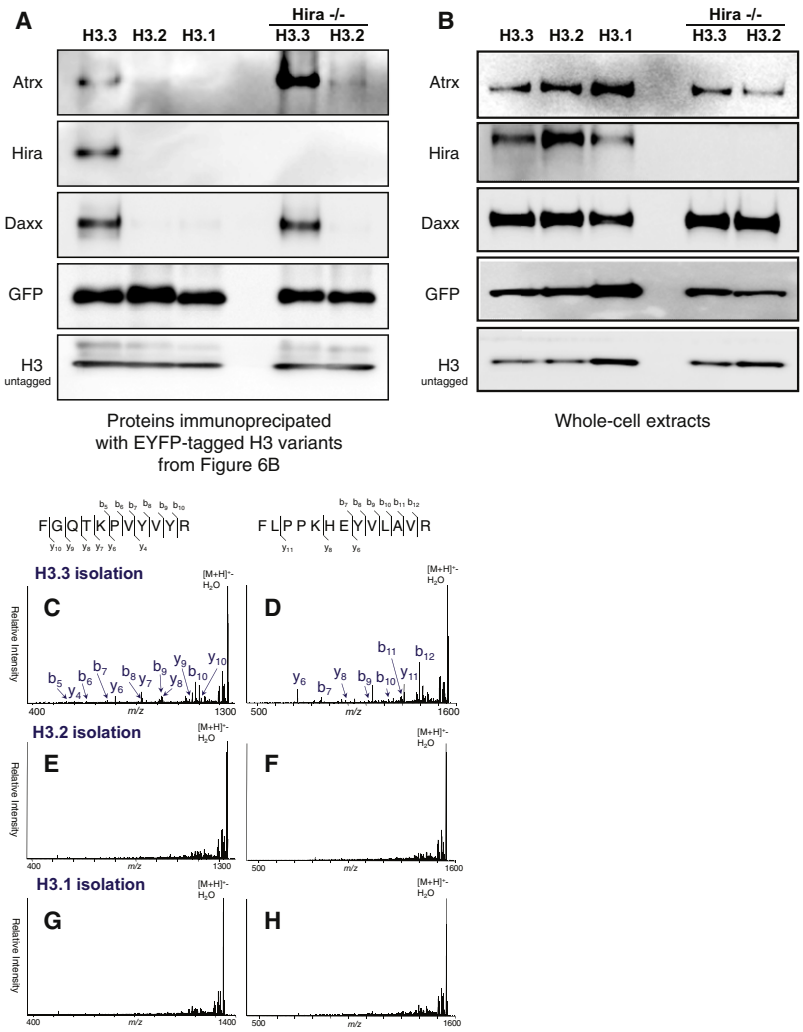

Figure S6. Specific and Hira-Independent Association of Atrx with H3.3, Related to Figure 6

(A) Immunoblots of immunoprecipitated proteins associated with EYFP-tagged H3 variants, as shown in Figure 6B.

(B) Immunoblots of whole cell extracts of ES cells used for immunoprecipitation in Figure 6B.

(C–H) Hypothesis-driven multistage mass spectrometry (Kalkum et al., 2003) was utilized to obtain a highly sensitive detection of specific peptides from proteins of interest, even if these peptide species could not be discerned in the primary matrix-assisted laser desorption/ionization MALDI MS analysis because of insufficient signal-to-noise. Even if Atrx peptides were not observed in the H3.2 and H3.1 samples at the MS level, their corresponding m/z values ([M+H]+) were selected, subjected to collision induced dissociation (CID) fragmentation, and analyzed using MALDI IT MS/MS analyses. The expected fragmentation pattern for the Atrx peptides was confirmed only in the sample isolated with H3.3 (A-B) as assessed by b and y ion fragments and the preferential cleavages C terminus of Glu and N-terminus of Pro residues. See Table S5 for a complete list of identified proteins and a summary of MS/MS analyses.

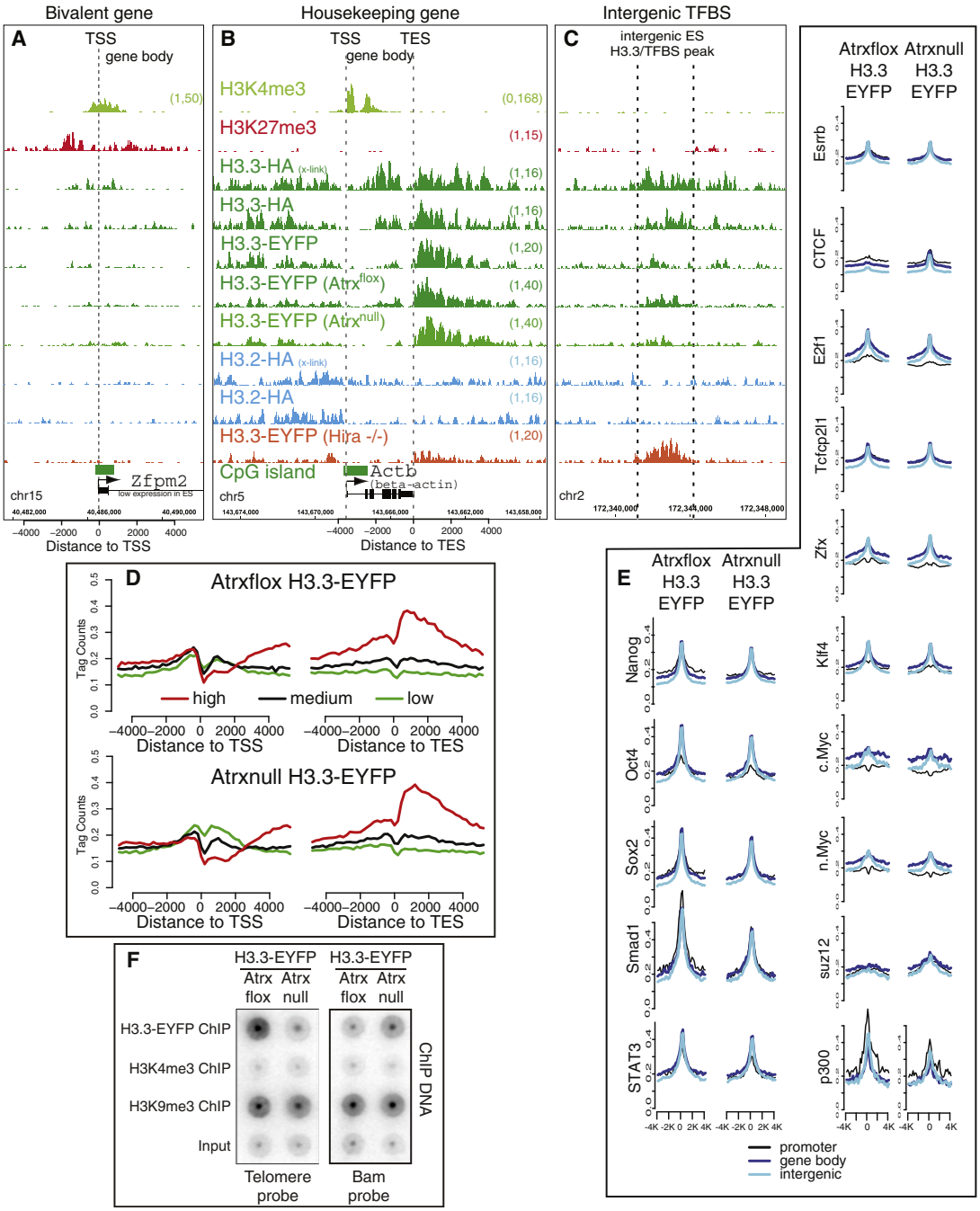

Figure S7. Atrx Is Not Required for Localization of H3.3 to Genes or Most Known Transcription Factor Binding Sites, but Is Required for H3.3 Localization to Telomeres, Related to Figure 7

(A–C) ChIP-seq profiles are shown at a bivalent gene, housekeeping gene, and intergenic regulatory region for H3.3 in the presence and absence of Atrx and Hira. All tracks are for native ChIP-seq, except for H3.3-HA and H3.2-HA crosslinking ChIP-seq tracks, indicated as "x-link." The scales for all tracks are the same in A-C except for H3K4me3, and are indicated in the right of panel A and B. Enrichment of H3.3 immediately around individual TSS is less appreciated in native ChIP-seq than crosslinking ChIP-seq, a phenomenon that is also seen in our genome-wide ChIP-seq profiles at TSS (Figure S4), and may be due to the labile nature of H3.3/H2A.Z nucleosomes in this region (Jin et al., 2009).

(A) ChIP-seq profiles at the H3K4me3/H3K27me3 bivalent gene Zfpm2 (also shown in Figure 2G).

(B) ChIP-seq profiles at the housekeeping gene Actb (also shown in Figure 2H).

(C) ChIP-seq profiles at an intergenic regulatory region (also shown in Figure 3F).

(D) Native ChIP-seq profiles of H3.3 in Atrxflox (top) and Atrxnull ES cells (bottom) as indicated across the TSS and TES for highly active (red), medium expressing (black), or low expressing (green) CpG rich genes, with data represented as in Figure 2 and Figure 4.

(E) Genome-wide profiles of H3.3 around previously described ES TFBS (Chen et al., 2008), and data analyzed as in Figure 3 and Figure 5.
(F) Dot blot with Sty11 telomeric probe (left) or control Bam repeat probe (right) of ChIP-seq DNA from Atrxflox H3.3-EYFP or Atrxnull H3.3-EYFP IPed with indicated antibody (GFP, H3K4me3, or H3K9me3) or Input DNA.